This is a repository copy of *Evaluation of in-cylinder endoscopic two-colour soot pyrometry of diesel combustion*.

Article:

Evaluation of in-cylinder endoscopic two-colour soot pyrometry of diesel combustion

Ruoyang Yuan [a],[*], Joe Camm [b],[1], Tristan Knight [c], Matt Parker [d], Suji Sogbesan [e], Edward Long [c], Vivian Page [f], Graham, K. Hargrave [c]

[a] Department of Mechanical Engineering, University of Sheffield, Sheffield S1 3JD, UK
[b] School of Engineering, Technology and Design, Canterbury Christ Church University, Canterbury CT1 1QU, UK
[c] Wolfson School of Mechanical, Electrical & Manufacturing Engineering, Loughborough University, Loughborough LE11 3TU, UK
[d] Rolls-Royce plc, Derby DE24 8BJ, UK
[e] BP plc, Pangbourne RG8 7QR, UK
[f] Caterpillar IPSD, Peterborough PE1 5FQ, UK

ABSTRACT

Flame temperature and soot concentration imaging was performed using endoscopic two-colour (2C) soot pyrometry to investigate the characteristics of in-cylinder diesel engine combustion processes and provide validation data for engine simulation and design. To appropriately interpret the 2C image results, this paper focuses on the uncertainty and challenges of the technique, the line-of-sight nature of the measurement and presents comparable information for validation exercises. A line-of-sight flame light intensity model was created to explore how the temperature T and soot concentration KL measured by the 2C technique can relate to non-uniform flame temperature and soot distributions. It was found that T and KL measured from the 2C technique were likely to relate differently to the actual distribution depending on where in the flame the measurement was taken and on assumptions made about the flame spatial structure. Assessment has been made of the range of the maximum and minimum flame temperatures (assumed to correspond to reaction zone temperature and flame centreline respectively) that are consistent with measured temperature T and soot concentration KL. The analysis of uncertainties, flame temperature and soot distribution along the line-of-sight, and image averaging allows for better quantitative comparison of 2C soot pyrometry images to CFD simulation, which increases confidence in simulation-driven engine development.

© 2022 The Authors. Published by Elsevier Inc. on behalf of The Combustion Institute.
This is an open access article under the CC BY license (http://creativecommons.org/licenses/by/4.0/)

1. Introduction

Great effort has been made over the years to understand the in-cylinder combustion process [1–3] in order to reduce pollutant emissions from transport while maximising performance; work which must be continued if future demands are to be met. In particular, for heavy-duty applications (including off-highway and heavy goods vehicles, stationary and marine engines) compression ignition combustion engines will maintain a significant role for the foreseeable future due to their reliability, good fuel economy and performance, range and cost. To design and develop low-emission engines that meet this need, understanding of the in-cylinder com-

bustion processes and the formation of emissions is vital. An attractive technique to achieve this insight is the use of multi-colour soot pyrometry to optically measure both flame temperature and soot formation; a useful approach which can be used to study both conventional and sustainable fuels. Based on Planck's law, this method measures the radiation from soot particles, which is temperature dependent and varies with wavelength. At thermal equilibrium, the ambient gas temperature is close to the soot temperature [4], therefore this method can provide a robust non-intrusive temperature measurement in combustion systems.

Soot pyrometry has been used successfully on a variety of fundamental burners [5–8] and combustion vessel reacting sprays [9] with excellent results and low uncertainty. Part of the success in the implementation of the two-colour (2C) technique with burners and flames is related to the flame axisymmetry, direct optical access, repeatability and stability, which have helped to overcome challenges due to the line-of-sight nature of the technique.

In these environments, complementary techniques, such as Laser-induced incandescence [10,11] and tomography [12–14] can be deployed to provide two-dimensional spatial distribution information about the relative soot concentrations and flame structure or provide for in situ calibration of the projected soot pyrometry results.

The two-colour soot pyrometry technique has also been used to obtain in-cylinder temperature and soot concentration (*KL*) distributions in a variety of optically-accessible engines [4,15-22]. Full diesel flame emission spectra have been collected using optical probes in large diesel engines in [15], using a range of fuels, demonstrating the location of emissions peaks from trace fuel components, such as sodium and potassium, which have been avoided in the present study. Previous work in [16] on single-sensor 2C pyrometry in a single-cylinder diesel engine has produced useful indicative results about diesel flame *KL* and temperature from a range of model fuels. The uncertainty analysis in this work is optimistic and has not evaluated the contribution to measurement uncertainties from factors considered in more recent work. This limits the value of the data from this experimental study for the quantitative validation of simulations. Sensor-integrated soot KL measurements were captured in [17] to investigate how the *KL* of the entire flame can be used to track soot oxidation in a heavy-duty engine under real conditions. However, typical 2C pyrometry methodology assuming a uniform flame was used, where the effects of soot or temperature variation along the line-of-sight were neglected. Partial filling of the view field by the flame or variability in the proximity of the flame to the optical probe were not accounted for. In [18], soot radiative emission was collected in a heavy-duty optical diesel engine, with light collected through an optical piston crown onto a photodiode. This was compared to corresponding CFD simulations. Local CFD cell soot and temperature predictions were summed in the vertical direction and then across the flame to create a model-average 2C $f_V L$ (proportional to *KL*). The presence of soot temperature gradients along the line-of-sight were predicted to produce greatest error to the integrated measurements collected by the photodiode, the authors noting that the magnitude of gradient is dependent on the operating condition. They recommended that 2C analysis be performed on simulation results, for subsequent comparison to experimental 2C data. An endoscopic imaging system was deployed by [19] to view inside the combustion chamber of a single-cylinder heavy-duty non-optical engine. Temperature and soot *KL* images were captured at a single condition to study NOx and soot formation with different injection strategies. Image-averaged flame temperature and *KL* were used to compare the strategies. Flame *T* and *KL* images were also presented to explain findings, although uncertainty analysis or analysis of the line-of-sight nature of the technique was not discussed. A useful study comparing steady-state and transient-state was performed, the endoscopic imaging being limited to transient-state because of window fouling. A similar more recent study using endoscopic soot pyrometry inside a heavy-duty engine is conducted in [20], with overall average flame temperature calculated from the 2C processed images at various crank angles, to explain the effects of injection strategy. Temperature and *KL* images are used for qualitative analysis. CFD results were presented but no analysis to account for temperature gradients within the simulated flames as recommended by [18] was carried out for validation of the simulation using the 2C images. A detailed study of 2C pyrometry in a direct injection natural gas–diesel piloted engine was conducted in [21] using a single cylinder optical engine, with the focus on making improvements for combustion conditions with lower soot radiance signal intensities. Uncertainty sources were surveyed and improvements suggested in solution algorithm, parallax correction for piston window viewing, image filtering, and matching of camera dynamic range to the experiment. Analysis of the errors from non-uniform temperature or soot distribution along the line-of-sight was not included in this work. With its simplicity and low cost compared with laser-based optical techniques, the 2C technique holds clear advantages for industrial engine combustion studies [18,19]. However, it is also evident that in-cylinder two-colour measurements are challenging due to limited optical access, often not orthogonal to the spray axis, which in turn impairs simultaneous application of complementary techniques. The transient, cyclically varying nature of the combustion process presents additional challenges in the interpretation of results. Due to these limitations, concern has been raised on the practical application of the two-colour technique for diesel flame analysis with its inherent line-of-sight nature [22]. This characteristic, whereby the 3-dimensional distribution of flame temperature and soot concentration are represented by either a single measured value or a 2-dimensional measured image, can result in significant uncertainty in the values recorded. To address this concern, it is of benefit to understand the uncertainties introduced by the unknown temperature and soot profiles present in practical engine flames.

Previous studies of the 2C method have addressed the non-uniform temperature distribution in flames and tried to quantify the effect on the measured temperature, known as the two-colour temperature or apparent temperature. For example, Matsui et al. [4] introduced the concept of flame layers at different temperatures, making a thorough study of the calibration, interpretation, statistics and limitations of the technique. However, their soot radiation measurements were through an aperture with a 3-mm field of view connected to a photomultiplier, meaning a picture of the overall flame could only be built up over many different experiments with different aperture positioning. This reduced the spatial resolution to around 3 mm in the diesel spray flame that they investigated. In addition, they utilised an assumed flame temperature distribution with peak temperature at the flame centreline. Payri et al. [22] extended this work to incorporate full flame imaging and a modelled flame temperature and soot distribution based on their knowledge of a diesel flame. They showed the discrepancy between average flame temperature and soot *KL* along the line-of-sight through a flame, and the 2C-derived temperature and *KL*, and additionally the dependence between 2C-derived *T* and *KL* measurements. Their experimental work was carried out using a single-hole injector, with extensive optical-access to the flame, perpendicular to the spray axis. They showed the variation in measured 2C temperature and *KL* with varying air temperature, air density and injection pressure, demonstrating further the relationship between *T* and *KL* 2C measurements

There are limited studies which incorporated a line-of-sight model in non-optical engines' 2C measurements and these were usually limited to point (light-integrated) measurements. A two-dimensional measurement of the temperature and soot distributions are still required, to add understanding of in-cylinder combustion processes, and to provide validation for the CFD development, which will further aid the design and delivering of low-emission high-efficiency engines. The focus of the work presented in this paper is to further understand the application of the two-colour method in the analysis of combustion within a production engine. The engine used has a multi-hole injector, with optical access to the in-cylinder combustion provided via an endoscope. In conjunction with the two-colour method, in-cylinder pressure was measured simultaneously. The results produced give insight into the flame structure and its development, while also providing an overall visualisation of the in-cylinder combustion process. To develop the two-colour soot pyrometry further as a useful, robust diagnostic for in-cylinder combustion analysis, the following factors have been carefully addressed: (1) analysis of uncertainty and sensitivity in relation to the measurement signal-to-noise ratio, optical setup and calibration; (2) systematic investigation of the uncer-
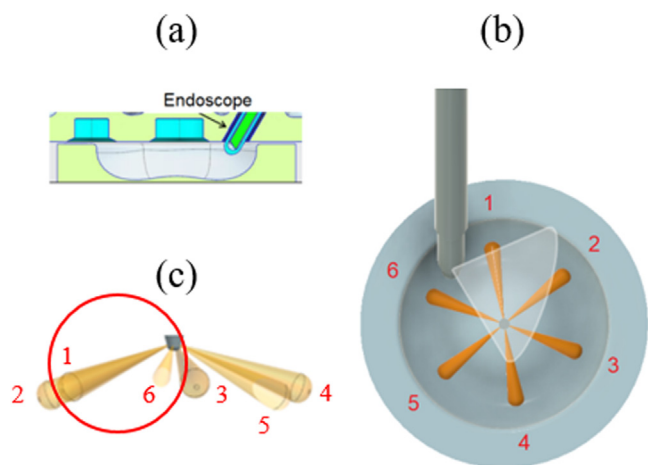
Fig. 1. (a) Endoscopic access point through glow plug hole, showing endoscope protruding into piston bowl; (b) position of the endoscope view cone (shaded area) focussing on one side of the combustion chamber; (c) view of the injector and plumes from the point of view of the endoscope aperture (red circle).

Fig. 2. Schematics of the endoscopic system for the engine tests: two achromatic lenses (A) were used to collimate the light; a 50:50 non-polarizing beamsplitter cube (B) and narrow bandpass filters (F) were used before the ICCD cameras fitted with Nikon lens.

tainty introduced by the line-of-sight nature of the technique with respect to anticipated structure of the measured diesel flame; (3) consideration of a method for appropriately averaging turbulent, cyclically-varying flames suitable for reduction to a 'mean' flame to allow comparison with simulation data and with other conditions. Within this work, a simple flame model was developed to further incorporate the effect of real-scale flame thickness and applied for the first time to the engine test data to back-calculate a plausible temperature and soot distribution. The measurements of T and KL that are identified as being located at different zones of the flame are compared to the simple flame model to understand which distributions of flame-temperature and soot-concentration along the line-of-sight are commensurate with the measured data. This process allows determination of possible flame temperatures, structures and temperature gradients within the flame for comparison with simulation data.

2. Methodology

2.1. Engine setup and endoscope access

This work concerns optical measurements captured from a firing four-cylinder thermodynamic engine, modified for endoscopic access to the combustion chamber in one of the cylinders. The engine was a Caterpillar diesel engine equipped with production hardware, including an engine control module (ECM) with a standard production calibration. Diesel fuel to BS EN 590 was supplied to the engine through a centralized fuel system. Data acquisition and image triggering control were performed using in-house real-time code written in LabVIEW, utilizing a National Instruments cRIO chassis with analogue and digital I/O modules installed. The optical diagnostics were conducted at several engine speeds and torques. In this paper, an intermediate load condition at 1400 rpm is used as an example case to address the 2C methodology.

Endoscopic access was obtained through modification of the glow plug hole of cylinder 1 (furthest from the flywheel). The axis of this hole is at 60° to the horizontal, as illustrated in Fig. 1(a). The endoscope system employed utilizes a 70° angle Karl Storz rigid endoscope with embedded cooling channel, mounting sleeve and pressure window provided by AVL for engine use. For the 2C measurements the endoscope view in Fig. 1(b) was adopted. The nominal view from the endoscope presented in Fig. 1(c) shows that there is overlap of plumes 1 and 2.
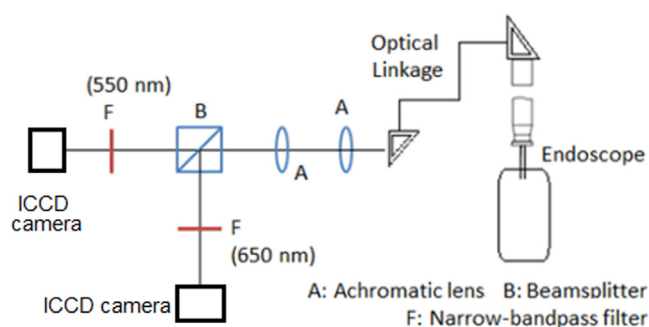
The in-cylinder pressure was recorded using a Kistler 6056A piezoelectric sensor mounted in the same cylinder via a second access point located between the intake ports.

2.2. Optics setup

The endoscopic measurement system setup is shown in Fig. 2. Two narrow bandpass filters (FWHM of 10 nm) were used with centre wavelength at $\lambda_1 = 550$ nm and $\lambda_2 = 650$ nm respectively for the 2C technique utilizing two 16-bit intensified ICCD cameras (Andor iStar). An in-house manufactured optical linkage was used to isolate the optics from the engine vibration and provide maximum light transmission out of the endoscope and into the collection system. A bespoke mounting system held the endoscope in a repeatable, user-defined position, allowing comparability of test runs.

The camera exposure time for the 2C measurement was set to 20 μs, allowing sufficient signal levels to be obtained while minimizing the movement of the flame during the exposure. At 1400 rpm, this time period corresponds to 0.17 °CA. The 2C technique was performed at a maximum frame rate of 4 Hz with data captured on a total of 50 individual cycles for each crank angle studied.

2.2.1. Technique calibration

The camera signal intensity, measured in counts at a certain pixel and denoted S_λ, is linked to the measurement of the local soot radiance, I_λ, by the transmission coefficient G_λ, such that $S_\lambda = G_\lambda I_\lambda$. The transmission coefficients of the detection system were obtained by imaging a spectral irradiance lamp (Quartz tungsten halogen (QTH) calibration light source, Newport, model number 63,976–200QC–OA, 200 W, NIST traceable calibration over a 300–2400 nm wavelength range). The experimental setup for this followed that shown in Spectral Irradiance, Oriel Product Training [23]. The irradiance from the QTH lamp was collected by the detection system at a distance of 0.5 m via a pinhole of diameter of 1.04 mm. The pinhole was placed in front of the endoscope aperture, since the endoscope aperture size was ill-defined, and positioned to give maximum transmitted light to the detection system. Calibration measurements used identical gain, gating setups, and camera conditioning (including camera temperature and background light levels) as used for the engine measurements due to the known non-linearity in intensified camera response. The lamp was operated under steady-state conditions. The calibrated coefficients were gathered at a range of irradiances relevant to local soot radiances expected in the engine measurements. These were generated with the lamp at its calibrated full-power level and utilizing absorptive neutral-density filters with measured attenuation.

2.3. Two-colour calculation method

Two-colour pyrometry utilises the intensity of radiation at two different wavelengths to infer the temperature of the emitting source. Therefore, to interpret the results from the images taken from the 2C technique, formulae for the radiation from a sooting flame were employed [4,5,16,24]. At wavelength λ, the soot radiance is given by

$$I_\lambda(\lambda, T) = \frac{\varepsilon_\lambda C_1}{\lambda^5}\left[\exp\left(\frac{C_2}{\lambda T}\right) - 1\right]^{-1} \tag{1}$$

where C_1, C_2 are known constants: $C_1 = 2hc^2 = 1.1910 \times 10^{-16}$ J m^2/s, and $C_2 = hc/k_B = 0.014388$ m K. The soot temperature, T, is assumed to very closely follow the temperature of the surrounding gas, as shown by Matsui et al. [4]. The soot emissivity ε_λ is given by

$$\varepsilon_\lambda = 1 - \exp\left(-\frac{KL}{\lambda^\alpha}\right) \tag{2}$$

where the wavelength dependence of the transmittivity of soot follows the work of Hottel and Broughton [5]. The factor KL is a measure of the flame optical thickness and can be related to soot concentration or number density with knowledge of soot optical properties and path length or volume through the flame L [24]. Alternatively, in some works a fixed or variable constant of proportionality is used to convert KL to $f_V L$, where f_V represents soot volume fraction [5,25]. In this work $\alpha = 1.39$ when the wavelength is measured in μm, as suggested by Hottel and Broughton for visible wavelengths and used by others (e.g. Payri 2007 [22]). In Zhao and Ladommatos [24], it is shown that the measured temperature value is insensitive to the exact value of α for visible wavelengths. To record the radiance intensities, two images of the same flame were captured, via two different wavelength filters, as shown in Fig. 2. The camera signal intensity (image pixel value) denoted as S_λ is a measure of local soot radiance I_λ and these are linked by $S_\lambda = G_\lambda I_\lambda$ with calibration factor G_λ as described in Section 2.2.1. Eqs. (1) and 2 can be combined and solved iteratively to produce images showing calculated two-colour temperature T_{2C} and soot KL_{2C} factor. An in-house developed image processing and calculation algorithm was developed and validated using the flame images from a well-established laminar gaseous diffusion flame against the literature on a replica of the standard co-flow burner (Yale co-flow burner [26]). Specifically, the two-colour temperature was calculated from the formula

$$T_{2C} = \frac{C_2\left(\frac{1}{\lambda_1} - \frac{1}{\lambda_2}\right)}{\left(\ln\frac{S_{\lambda2}}{S_{\lambda1}} + \ln\frac{G_{\lambda1}}{G_{\lambda2}} + \ln\frac{\varepsilon_{\lambda2}}{\varepsilon_{\lambda1}} + 5\ln\frac{\lambda_2}{\lambda_1}\right)} \tag{3}$$

Initially, the ratio of emissivities is taken as equal to unity. With the first estimated temperature image, the blackbody radiation $I_{BB,\lambda}$ can be found, which enables KL_{2C} to be calculated from the expression

$$KL_{2C} = -\lambda^\alpha \ln\left(1 - \frac{I_\lambda}{I_{BB,\lambda}}\right) = -\lambda^\alpha \ln\left(1 - \frac{S_\lambda}{G_\lambda I_{BB,\lambda}}\right) \tag{4}$$

This allows the emissivity at each wavelength to be updated and the temperature to be recalculated from Eq. (3). This process is iterated until convergence of T_{2C} to within 0.1 K and KL_{2C} to within 0.001 at both wavelengths. In this way, only for KL_{2C} is absolute calibration needed. For T_{2C}, only the relative calibration factor $G_{\lambda1}/G_{\lambda2}$ is required to be measured during calibration, which has a lower uncertainty value.

2.4. Measurement uncertainties

Measurement uncertainties for the two-colour measurement technique applied to a practical engine diagnostic system are assessed and quantified where possible in this section. The error due

to the wall or spray reflection and window soot deposit is small, as discussed in [4,22], such that the effect on the 2C processed T and KL is negligible (analysis in [4] for linear multiple reflections of flame radiance off detector optics and combustion chamber walls concluded an error of 10 K was possible if the contribution from these multiple reflections was ignored, based on 2000 K flame temperature). The typical ratio between the instantaneous radiation signal level (after the background subtraction and image de-speckling) and the average noise-signal of the acquisition is in between 35:1 and 6:1. The noise-signal in this case was quantified as the average signal in non-flame regions as captured by the intensified camera during experiments, which was calculated during image processing. This noise-signal includes the background offset present in the camera even with zero light level, non-flame light captured either from the experimental room or diffuse reflections from the combustion chamber, and any unidentified camera noise present when the camera is in operation. Shot-to-shot variation of the intensified camera response when measuring a steady light source (the calibration lamp described in Section 2.2.1) is less than 4% based on a set of 50 calibration images acquired at 4 Hz. This effect is not transferred to the calibration factors, due to averaging over the 50 images. The steady light source used was the calibration lamp, whose calibration uncertainty is 1.7% and whose anticipated intensity drift is negligible according to the manufacturer [27]. The measurement layout of the calibration procedure performed contributes a 4% uncertainty in G_λ. The uncertainty in G_λ leads to 4% uncertainty in the absolute intensity measurement of KL in the experimental setup. The calibration took account of the slight nonlinearity between incident light intensity and camera output, which was more apparent at lower signal values. The factor $G_{\lambda1}/G_{\lambda2}$ used in Eq. (3) was measured directly from the calibration experiment, therefore the uncertainties from lamp drift and the calibration setup measurement are greatly reduced. The contribution to this factor is taken as $\sqrt{2} \times 1.7\% = 2.4\%$. Maximum error due to finite wavelength-bandwidth is estimated as 10 K in T and 2% in KL [22]; uncertainties in the centre wavelength values are negligible compared to the other measurement uncertainties considered.

Errors due to the displacement of flame edges during the exposure time can be substantial in quantifying KL at the flame edge (i.e. an estimated 15% at 10 °CA ATDC), but this is calculated to have small direct effect in T. Correct alignment of the two images at the two wavelengths is important to give accurate results. This is done via a cross-correlation programme to reduce the error in the images' alignment. Assuming that there exists a maximum of a one-pixel misalignment due to this autocorrelation, there is a root mean square difference up to 70 K or 3.5% at 2000 K. This was found by manually shifting one of the raw soot images at the conditions studied in this paper. Errors with the line-of-sight nature are discussed in the results section.

Error analysis has been performed to translate these measurement uncertainties into expected uncertainties in the final T and KL values. For the temperature calculated from Eq. (3), uncertainties arise initially from the soot image ratio $S_{\lambda2}/S_{\lambda1}$ and from the calibration factor ratio $G_{\lambda1}/G_{\lambda2}$. For the soot image ratio, the uncertainties from each of the two images are a maximum of 4% (the shot-shot variation reported earlier) but these are independent. Therefore, the overall fractional uncertainty in $S_{\lambda2}/S_{\lambda1}$ is $\sqrt{2} \times 4\% = 5.6\%$. The fractional uncertainty in the calibration factor ratio was measured directly as 2.4%. The expected uncertainty in T due to these two contributing uncertainties can be calculated from the following equation [28]:

$$\delta T = \sqrt{\left(\frac{\partial T}{\partial\left(\frac{S_{\lambda2}}{S_{\lambda1}}\right)}\delta(S_{\lambda2}/S_{\lambda1})\right)^2 + \left(\frac{\partial T}{\partial\left(\frac{G_{\lambda1}}{G_{\lambda2}}\right)}\delta(G_{\lambda1}/G_{\lambda2})\right)^2} \tag{5}$$

This results in the expression shown in Eq. (6):

$$\left| \frac{\delta T}{T} \right| = \frac{T}{C_2 \left(\frac{1}{\lambda_1} - \frac{1}{\lambda_2} \right)} \sqrt{ \left(\frac{\delta (S_{\lambda 2}/S_{\lambda 1})}{(S_{\lambda 2}/S_{\lambda 1})} \right)^2 + \left(\frac{\delta (G_{\lambda 1}/G_{\lambda 2})}{(G_{\lambda 1}/G_{\lambda 2})} \right)^2 } \quad (6)$$

This equation means that the fractional uncertainty is dependent on the temperature measured by the technique. At 2000 K, $|\delta T/T| = 3\%$ or 60 K and at 2500 K, $|\delta T/T| = 3.8\%$ or 95 K, and at 3000 K, $|\delta T/T| = 4.5\%$ or 135 K.

The uncertainty in the measurement of KL can be calculated in a similar way. First, the uncertainty in emissivity ε_λ is considered, where $\varepsilon_\lambda = S_\lambda / G_\lambda I_{BB,\lambda}$ and can be calculated from the following equation:

$$\frac{\delta \varepsilon_\lambda}{\varepsilon_\lambda} = \sqrt{ \left(\frac{\delta S_\lambda}{S_\lambda} \right)^2 + \left(\frac{\delta G_\lambda}{G_\lambda} \right)^2 + \left(\frac{\delta I_{BB,\lambda}}{I_{BB,\lambda}} \right)^2 } \quad (7)$$

The uncertainty in the black body radiance can be derived from the formula:

$$I_{BB,\lambda}(\lambda, T) = \frac{C_1}{\lambda^5} \left[\exp \left(\frac{C_2}{\lambda T} \right) - 1 \right]^{-1} \approx \frac{C_1}{\lambda^5} \exp \left(-\frac{C_2}{\lambda T} \right) \quad (8)$$

This approximate expression is accurate for light in the visible wavelengths at high temperatures and leads to a fractional uncertainty given by:

$$\left| \frac{\delta I_{BB,\lambda}}{I_{BB,\lambda}} \right| = \frac{C_2}{\lambda T^2} \delta T = \frac{C_2}{\lambda T} \left| \frac{\delta T}{T} \right| \quad (9)$$

This is in fact independent of temperature (combining Eq. (6) and Eq. (9)) and related only to the errors in S_λ and G_λ. Unfortunately, the fractional uncertainty in the black body radiance is quite high at 34% at 2500 K as calculated from Eqs. (6) and 9, which is not surprising since a change in temperature of around 130 K will cause a factor of two change in the black body radiance at the wavelengths and temperatures encountered. Since the uncertainty in black body radiance is dominant compared to those in signal level and calibration constant (each around 4%), the fractional uncertainty in emissivity is also up to 34%.

The emissivity uncertainty will propagate through to KL, where since $KL = -\lambda^\alpha \ln(1 - \varepsilon)$, the uncertainty in KL can be calculated as

$$\delta KL = \frac{\lambda^\alpha \varepsilon}{1 - \varepsilon} \left| \frac{\delta \varepsilon}{\varepsilon} \right|, \quad \frac{\delta KL}{KL} = \frac{\varepsilon}{(1 - \varepsilon) \ln(1 - \varepsilon)} \left| \frac{\delta \varepsilon}{\varepsilon} \right| \quad (10)$$

As $KL \to 0$ and $\varepsilon \to 0$, then $\frac{\delta KL}{KL} \to \frac{\delta \varepsilon}{\varepsilon}$. At large KL values, that is with emissivity approaching unity, the absolute uncertainty in KL will increase greatly. The effect of this, coupled with the high uncertainty in emissivity, is that the uncertainty in KL becomes impractical at high values of KL, as demonstrated in Fig. 3. Taking $\frac{\delta \varepsilon}{\varepsilon} = 34\%$, the fractional uncertainty $\frac{\delta KL}{KL}$ can be calculated as 34% at $KL \to 0$ rising to 97% at $KL = 1.0$. In addition, the accuracy of the absolute calibration has little impact on the KL uncertainty due to the dominant effect of the black body radiance uncertainty.

2.5. Flame light intensity model (FLIM)

2.5.1. Line-of-sight flame light intensity model

Each pixel on the converged T_{2C} image represents a flame temperature based on the contribution of soot radiation along the line-of-sight from the endoscope through the flame; previous works have discussed how this 'two-colour' temperature relates to the mean flame temperature or the actual temperature distribution. It is usually found that the two-colour temperature is higher than the spatial mean temperature and higher still than the mass-weighted temperature [4,22]. Therefore, to further understand the T_{2C} measurements and provide insight into its line-of-sight integration, a
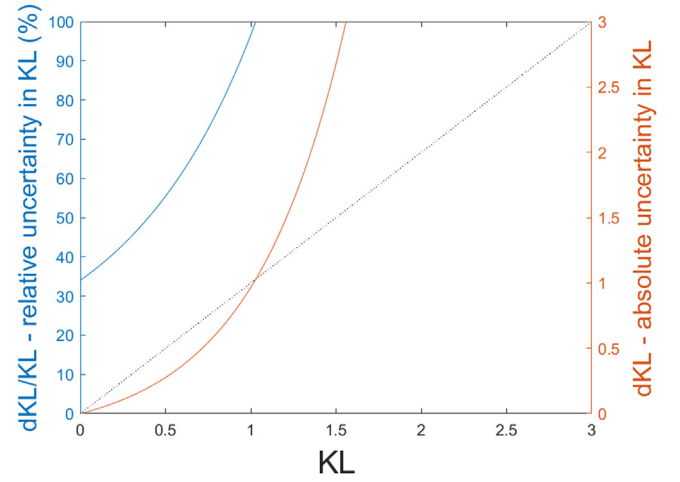

Fig. 3. Absolute and relative uncertainty in KL resulting from 34% uncertainty in black body radiance, calculated at 650 nm. The relative uncertainty reaches 100% of KL at around $KL = 1.03$.

model of emitted light intensity from a flame with non-uniform temperature and soot concentration was created.

For the recorded images, the light incident on a given camera pixel is the superposition of contributions of light from radiant soot along the corresponding ray through the flame. Due to the concentration of soot particles generated within the flame, the light emitted by soot at one part of the flame is attenuated by further soot particles between the original soot particle and the aperture of the optical system, in this case the endoscope tip inside the combustion chamber. Since the endoscope aperture has a finite size, it collects light from the soot at a given location over a finite solid angle. Each ray in the cone of rays from each soot particle will travel through different parts of the flame and be subject to a different rate of attenuation. However, in the experiments considered in this paper, the aperture size (~3 mm) is much smaller than the assumed distance to the soot particle (taken as 30 mm). Therefore, for the purposes of comparison to a simplified model of a diesel flame, the light paths will be assumed to be appropriately represented by a straight line from soot to endoscope tip and thus emission and attenuation need only be considered along this path.

The equations used in the developed model are adapted from those presented in [4,22]. In [22] a simplified diesel turbulent jet flame model was presented with axisymmetric, steady state flame temperature distributions based on the local mixture fraction and jet velocity, assuming unity Schmidt and Lewis numbers. Soot concentrations were not calculated but either a uniform or piece-wise linear distribution of soot concentration was imposed. These combinations of modelled temperature and soot concentration were then analysed to calculate what the two-colour temperature and KL would be if such a flame was investigated using the two-colour method. This result was compared to flame images from a single-hole diesel injector. The optical axis in [22] was normal to the spray axis, whereas in the current study the flame is observed from a range of oblique angles due to the nature of the multi-hole fuel injector and the specific optical access available to the combustion chamber.

Following the work [4,22], the flame is discretized into n thin layers along the line-of-sight; $n = 1000$ has been chosen for this work. At each layer of thickness $\Delta l = L/n$, the soot has a temperature of T_i and a soot concentration factor $k_{soot,i}$. The factor $k_{soot,i}$ is proportional to the soot concentration, and the product $k_{soot,i} \Delta l$ would be equal to the KL factor for that flame layer alone. Thus, a temperature and soot concentration distribution along the line-of-sight of a hypothetical flame can be built up by adding together

these layers. The radiance from each layer i is then:

$$I_{\lambda,i} = \varepsilon_{\lambda,i} I_{BB,\lambda,i} = \left[1 - \exp\left(-k_{soot,i} \frac{\Delta l}{\lambda^{\alpha}} \right) \right] C_1 \lambda^{-5} \left[\exp\left(\frac{C_2}{\lambda T_i} \right) - 1 \right]^{-1} \tag{11}$$

Assuming each soot layer to be a grey body (with an emissivity less than unity and the same at all wavelengths) and to obey Kirchhoff's Law, the transmissivity through each layer will be $C_{\lambda,i} = 1 - \varepsilon_{\lambda,i} = \exp(-\frac{k_{soot,i}\Delta l}{\lambda^{\alpha}})$, and the total detected radiance received from the n layers will be:

$$I_{\lambda} = \sum_{i=1}^{n} \left[\left(1 - C_{\lambda,i} \right) C_1 \lambda^{-5} \left(\exp\left(\frac{C_2}{\lambda T_i} \right) - 1 \right)^{-1} \prod_{j=i+1}^{n} C_{\lambda,j} \right] \tag{12}$$

In a flame with uniform soot concentration and hence uniform k_{soot} distribution, $C_{\lambda,i} = \exp(-\frac{KL}{n\lambda^{\alpha}})$ and is constant throughout the flame. Eq. (12) reduces to Eq. (1) when T_i and $k_{soot,i}$ are uniform. Light attenuation by soot layers allows a non-uniform soot and/or temperature distribution to radiate the same I_{λ} as another uniform distribution at certain temperature and soot levels, meaning this uniform temperature and KL are the two-colour technique values for that non-uniform distribution. This is equally applicable to flames of any overall thickness L, with the distribution of k_{soot} simply stretched or contracted to suit. However, as L is increased in a practical flame, it may be that the near edge of the flame is brought closer to the detector and the far edge becomes further away. Due to the inverse square law, soot that is physically closer to the detector contributes a greater proportion to the irradiance received by the detector. This feature acts in addition to the attenuation of soot radiance that travels through the flame. In this work, the effect of real-scale flame thicknesses is incorporated into Eq. (12) by including a factor proportional to the solid angle that is subtended by the detector at each soot layer i, giving the equivalent detected radiance accounting for the inverse square law:

$$I_{\lambda,\ ISL} = \sum_{i=1}^{n} \left[\left(\frac{S_{CL}}{S_{CL} - \frac{L}{2} + i\Delta l} \right)^2 \left(1 - C_{\lambda,i} \right) C_1 \lambda^{-5} \left(exp\left(\frac{C_2}{\lambda T_i} \right) - 1 \right)^{-1} \prod_{j=i+1}^{n} C_{\lambda,j} \right] \tag{13}$$

where S_{CL} is the distance to the flame centreline, taken here as 30 mm. The effect of accounting for the flame thickness is investigated in Section 2.5.2, with evaluation of the effect on measured values and measurement uncertainty discussed.

Given a distribution of temperature T_i and soot concentration $k_{soot,i}$, Eq. (12) or 13 can be used to reproduce what the two-colour method would provide as a temperature and KL measurement. Conversely, given a combination of temperature T_{2C} and soot factor KL_{2C} measured with the two-colour method, and a parameterized distribution shape for the practical temperature and soot concentration distribution, families of temperature and soot concentration distribution can be found that result in the same two-colour T and KL values. However, the soot and the temperature profiles cannot be calculated simultaneously; prescribing a range of k_{soot} distributions allows the temperature distribution to be calculated for each k_{soot} distribution. The calculated T_{2C} is typically weighted towards the hottest temperature in the distribution which has a greater contribution to the light emission.

Figure 4(a) presents a visualization of idealized, self-similar flame temperature and soot concentration (k_{soot}) profiles, along line-of-sight coordinate l, following the work [17,22]. For these non-uniform distributions, the actual KL value of the flame along that line-of-sight would equal $\int_{-L/2}^{L/2} k_{soot} dl$, which will be different to the value measured from the two-colour system due to the non-

linear contribution of KL in the governing equations, see Eq. (12), as also demonstrated in [22].

Due to the fixed position of the endoscope collection optic, which is in close proximity to the flame in the combustion chamber, the view of the flame is through a variety of oblique angles as demonstrated in Fig. 4(b). View-paths through the flame at different positions along the penetrating plume may have a longer L as shown in Fig. 4(b), meaning that for a given KL the corresponding local or averaged soot concentration will be smaller. Due to the self-similar radial profiles assumed, the longer or shorter line-of-sight paths through the flame at non-normal viewing angles will exhibit a skewed temperature and soot concentration profile shape with the centreline temperature and soot concentration values skewed to the near or far side.

The selected families of distribution of T and k_{soot} used in this work and demonstrated in Fig. 4 were based on the current understanding of the structure of conventional diesel combustion flames. In the developed flame, temperature is expected to be at a peak towards the flame edge, where the equivalence ratio approaches 1. There is expected to be soot throughout the flame, with a reduced concentration towards the leaner, high temperature edges and higher concentrations towards the flame centreline, where the mixture is richer, inhibiting soot oxidation and promoting fuel pyrolysis, as demonstrated by ECN (Engine Combustion Network) laser-induced incandescence (LII) and soot extinction measurements [3,29]. Recent simulation work [30] predicted a soot volume fraction peak off the centreline, which has been included in the five-point model described in Section 3.4 alongside a flat central soot concentration, to calculate possible distributions of T and KL from the measurement data T_{2C}, KL_{2C}.

2.5.2. FLIM demonstration

To show the use of FLIM on flame distributions, a symmetrical three-point distribution was imposed for temperature, as expressed in Eq. (14), with a maximum temperature at the flame edge corresponding nominally to stoichiometric conditions, outside of which the soot concentration is reduced to zero.

$$\begin{cases} T = T_c + (T_e - T_c)\frac{|r|}{R}, & (0 \le |r| \le R) \\ KL = KL_c = KL_e \end{cases} \tag{14}$$

in which subscript e and c denotes the edge and centre respectively, R is the distance between the flame edge and flame centre, and r is the radial coordinate. For this initial demonstration, the soot concentration throughout the flame is set to be uniform, so that $KL = k_{soot}L$. In Fig. 5(a) are shown results from calculations using Eq. (12) with T_{2C} set to 2325 K and KL_{2C} of 0.3. Each temperature profile in Fig. 5(a) gives the same T_{2C} and KL_{2C}. As can be seen in Fig. 5(a), a range of the uniform KL value from 0.3 to 0.75 produces a variation of only 85 K in flame edge temperature but gives a variation of 900 K in flame centre temperature. Each distribution, if representing a real flame measured with the 2C system would result in the same value of $T_{2C} = 2325$ K and $KL_{2C} = 0.3$. With higher values of KL, the flame centre temperature may become unrealistically low (900 K, taken as the estimated pre-combustion temperature), providing an upper bound for the actual KL (in this example, a bound of 1.2, indicated by Fig. 5c) and hence k_{soot} value that could be expected from such a flame, given the two-colour measurements that were taken from it.

To assess the effect of finite flame thickness and the inverse square law on the feasible temperature distributions at this condition, results are shown in Fig. 5(b) from calculations using Eq. (13), with $S_{CL} = 30$ mm and flame thickness $L = 10$ mm. It can be seen that a uniform KL value equal to the measured KL_{2C} now requires a non-uniform temperature distribution varying about the T_{2C}. In ad-
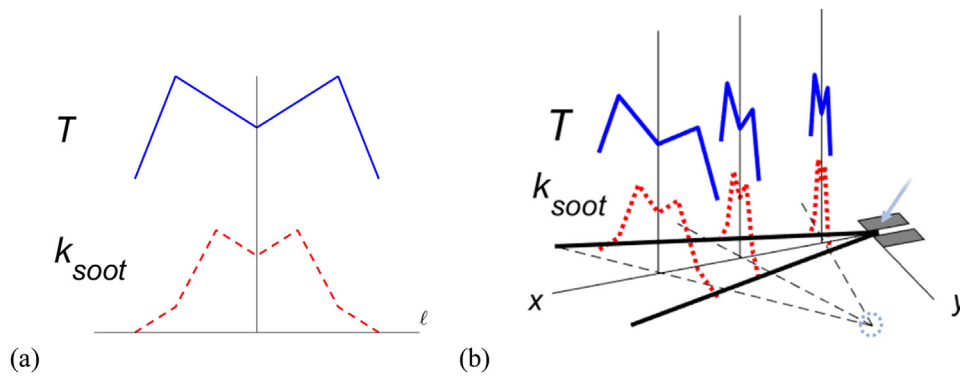
Fig. 4. Schematic temperature and soot *KL* distribution: (a) 2-D section through the flame (b) 3-D representation showing similar distributions through different parts of the flame, with different viewing angles to the endoscope collection optics. Arrow points at the injector hole, dotted circle marks the location of the endoscope aperture, and dashed lines indicate the different line-of-sight coordinates *l*.
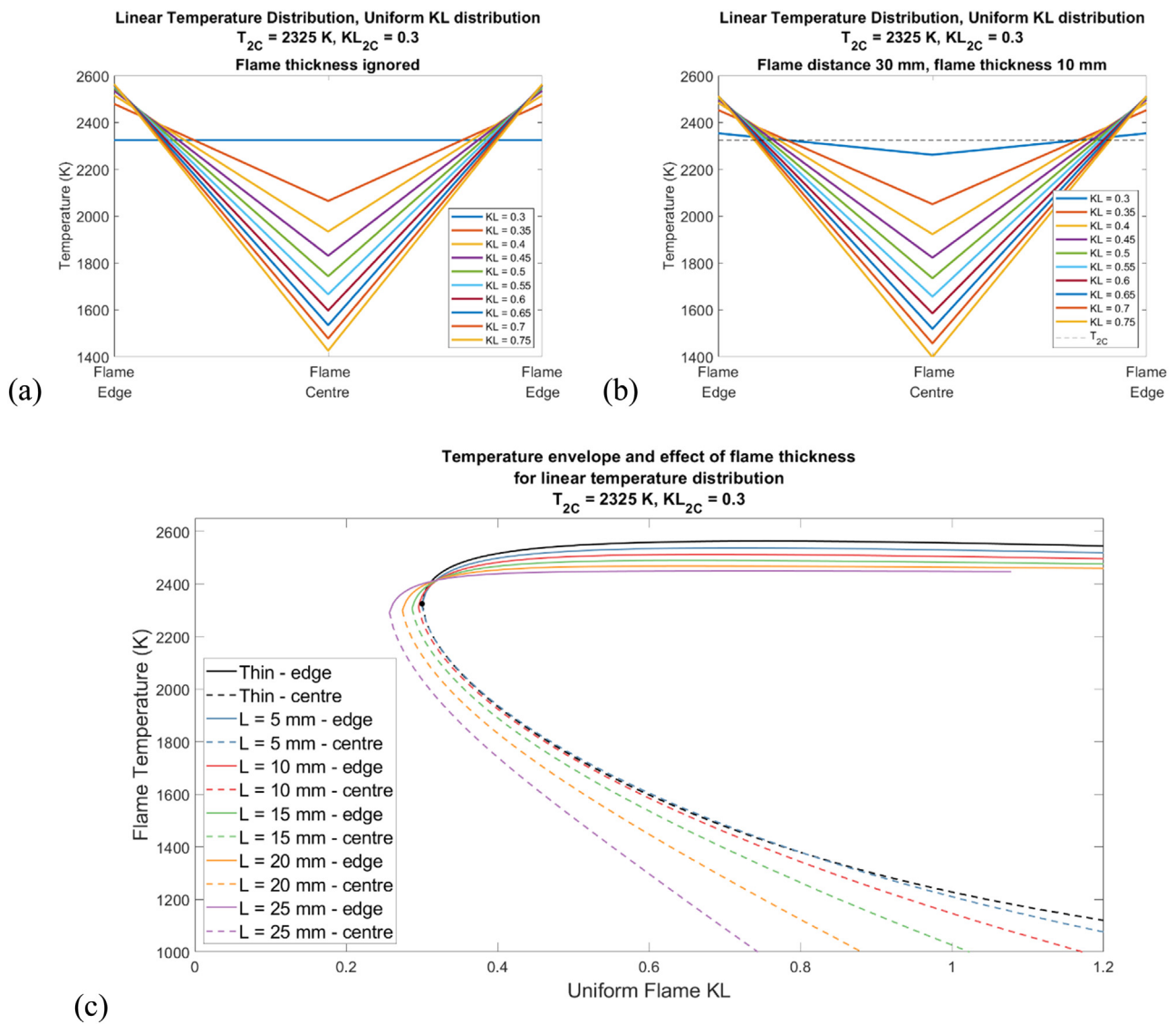
Fig. 5. Calculated three-point temperature profiles that result in the same T_{2C} (2325 K, solid horizontal blue line) and the KL_{2C}(0.3), with a range of imposed uniform *KL* values (Eq. (14)), (indicated in the legend): (a) with flame thickness ignored, (b) with a flame thickness of 10 mm. (c) Flame edge and centre temperatures required from the three-point temperature profile that result in the T_{2C} of 2325 K and KL_{2C} of 0.3, as a function of imposed *KL*, for thin flames and given thicknesses. With increasing flame thickness, the interval of flame temperatures is lowered and the minimum feasible imposed *KL* reduces below 0.3.

dition, temperatures throughout the distribution including at the edge and at the centre are reduced when the flame thickness of $L = 10$ mm is taken into account. This may be explained by the fact that the near edge of the flame, which is at the highest temperature due to our assumed temperature distribution shape and is therefore the brightest part of the flame, has effectively been brought closer to the detector than when the flame thickness was ignored. Therefore, its contribution to overall detector irradiance is further increased. Due to soot attenuation, the near edge of the flame contributes the most to the overall irradiance, so to achieve the same irradiance at the detector and hence the same two-colour measurement, the flame must be cooler overall. This effect increases as the flame thickness is increased.

The effect of the actual uniform KL value in the flame and the effect of the finite flame thickness are shown in Fig. 5(c). This plot shows that, for the modelled flame, the values of edge temperature (solid lines) do not vary significantly as the KL factor changes. Therefore, uncertainty in flame edge temperature caused by poor knowledge of the real soot concentration is relatively low. Whereas, the values of centre temperature (dashed lines) decrease significantly as KL is increased. Therefore, significant uncertainty in flame centre temperature is caused by lack of knowledge of the real soot concentration. The reduction in the flame edge temperature at a given KL due to increase of the flame thickness up to 15 mm was no more than 75 K at this condition. The effect of flame thickness on flame centreline temperature was lower at low KL but increases rapidly as KL increases. The effects of flame thickness variations will not be explored further in this work.

In Section 3.4, the FLIM is applied to the in-cylinder T and KL data from the 2C measurements, to back-calculate a plausible flame distribution. The model used is a five-point distribution for T and $k_{soot}L$, as expressed in Eq. (15), which will be further discussed in Section 3.4. The subscript q refers to the values chosen for $r = \frac{R}{2}$. Note that Eq. (15) becomes Eq. (14) when $T_q = (T_e + T_c)/2$.

$$\begin{cases} T = T_c + (T_q - T_c)\frac{2|r|}{R} \\ k_{soot}L = (k_{soot}L)_c + \left[(k_{soot}L)_q - (k_{soot}L)_c\right]\frac{2|r|}{R} \end{cases}, \quad \text{for } (0 \le |r| \le R/2)$$

$$\begin{cases} T = T_q + (T_e - T_q)\left(\frac{2|r|}{R} - 1\right) \\ k_{soot}L = (k_{soot}L)_q + \left[(k_{soot}L)_e - (k_{soot}L)_q\right]\left(\frac{2|r|}{R} - 1\right) \end{cases}, \quad \text{for } (R/2 < |r| \le R)$$

$$(15)$$

3. Results and discussion

In this section, instantaneous soot pyrometry measurement images are presented, captured from the heavy-duty engine endoscopic access system. These results are put into context within the in-cylinder diesel combustion process by comparing them to the cylinder pressure and mean apparent heat release rate (AHRR), in conjunction with the injection and combustion event timings in Section 3.1. The distributions of instantaneous temperature (T_{2C}) and soot KL_{2c} that have been measured are analysed, with consideration to where in the flame T_{2c}-KL_{2c} pairs are located and how the measured values compare to measurement uncertainty and signal-noise ratio (Section 3.2). Appropriate methods of averaging the data are presented in order to create an ensemble-averaged soot pyrometry measurement for comparison to other conditions or to simulation results. The spatially-averaged temperature and soot data processed from the 2C method are plotted together to show the overall temporal development of the key combustion parameters in Section 3.3. Finally, measured T_{2c}-KL_{2c} pairs are compared to results from the FLIM to give estimates of the range of potential flame temperature and soot concentration distributions that are commensurate with the 2C data from the in-cylinder diesel
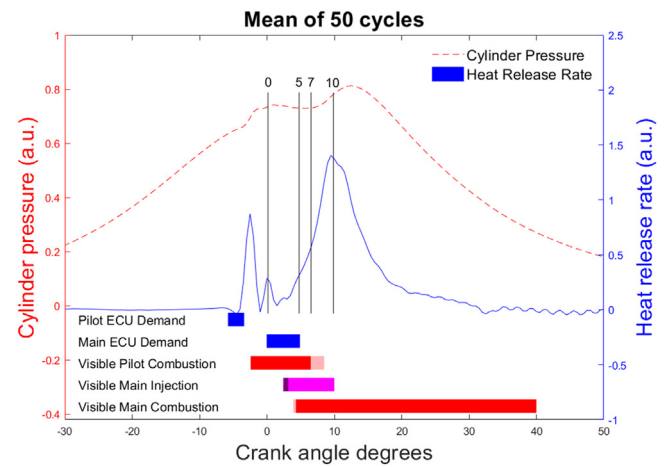

Fig. 6. Simultaneously acquired cylinder pressure and apparent heat release rate. Vertical lines indicate the corresponding crank angles at which the two-colour images were captured.

flame measurements. These findings are discussed in relationship to the 2C measurements uncertainties at the end of the Section 3.

3.1. Two-colour images

Images captured with the engine running at 1400 rpm at an intermediate load condition are discussed here. The mean pressure trace and associated AHRR from this condition are shown in Fig. 6, averaged from 50 cycles; labelled bars underneath the graph indicate the combustion events and injection timing. The AHRR is a net heat release rate and is unsmoothed. An example raw soot image is shown in Fig. 7(a), taken at 7 °CA, where high intensity flame soot radiation is observed around the visible spray of the plume 1 (boundaries illustrated by red lines), and propagating towards the pistol bowl (indicated by the dash line). An image series of instantaneous raw soot images taken at 550 nm is shown in Fig. 7(b), demonstrating the progression of the combustion event. These images are taken at random cycles. Firstly, the pilot combustion is seen over crank angles −2 to 2. The main combustion is seen to begin at 4 °CA and from then the plume is seen to propagate into the bowl, increasing in intensity, and peaking at 7 °CA. Next, the head of the plume passes beyond the edge of the field of view and the intensity appears to decrease. The reduction in intensity is against what is observed in the heat release, Fig. 6, caused by the main intensity of the plume being outside of the endoscope view. The intensity appears to peak again at 12.5 °CA as the flame is brought back into the view by the swirl. Instantaneous examples of the processed T_{2c} and KL_{2c} images are shown in Fig. 7(c-e), for image timings of 0 °CA, 5 °CA, 7 °CA and 10 °CA ATDC. Cycle-to-cycle variation is seen from the instantaneous images. Considering the engine heat release diagram in Fig. 6, the images at 0 °CA are of the pilot combustion plumes, whereas the other timings shown occur during the main combustion event, with 10 °CA ATDC being around the time of peak heat release rate and the end of the fuel injection event. The injector is located to the top right of the images. Since the injector has six equally spaced holes, the three right-hand plumes (4 to 6 in Fig. 1) are largely missing from the image. The data from the centre towards the bottom left of the images represents the plume nearest to the endoscope (plume 1) and this is mostly continuous with the light from the adjacent plume (plume 2), whose axis is 32° beyond normal to the viewing axis from the endoscope. Looking at the images from the 10 °CA timing, the region with higher KL_{2c} values at the top centre represents the farthest plume around (plume 3), which is broadly travelling away

(a)
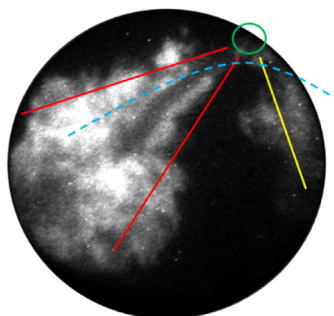
(b)
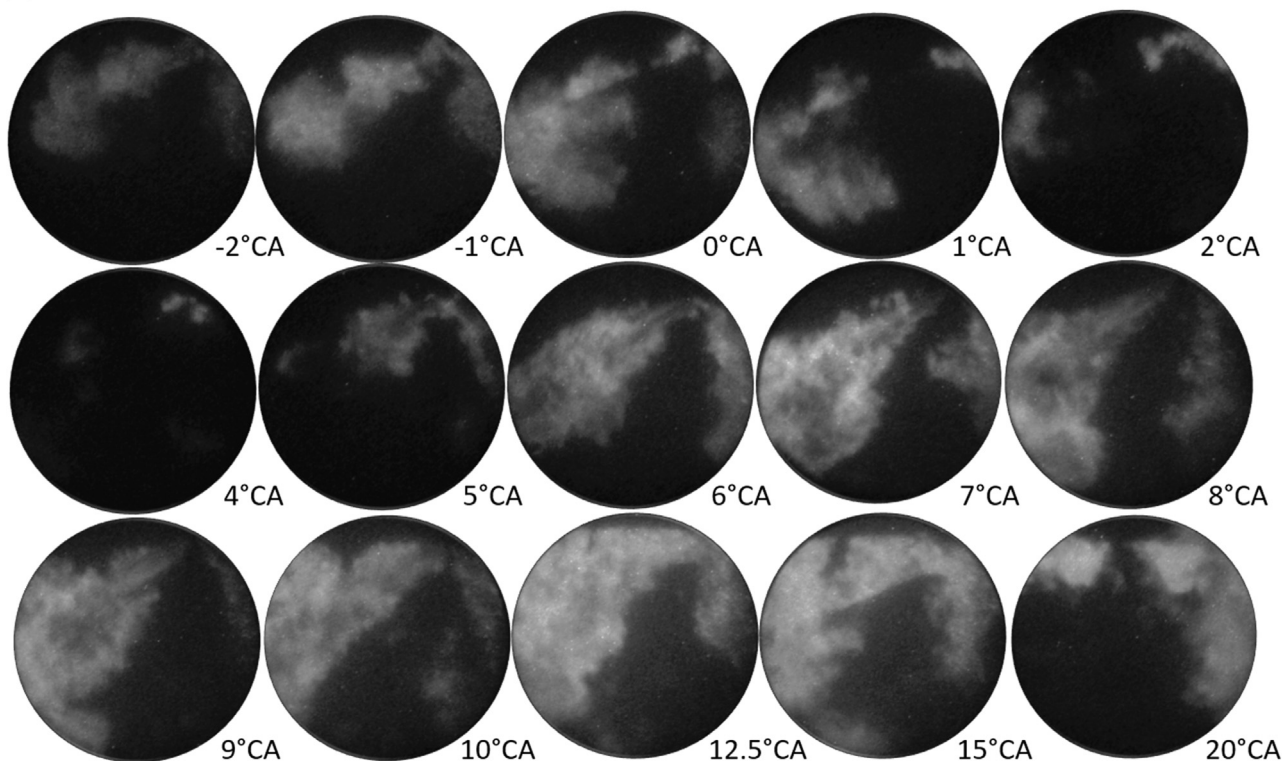
Fig. 7. (a) An example raw soot image captured (at 7 °CA, filtered at 550 nm) from one of the ICCD cameras, superimposed by illustration lines and curves: red – indicating the boundaries of plume 1, yellow – boundary of plume 3, green – location of the spray injectors, and blue – location of the piston bowl. (b) An image series showing an example of the combustion event: −2 °CA to 20 °CA, filtered at 550 nm. (c, d, e) Three examples of instantaneous 2C images at 0 °CA, 5 °CA, 7 °CA and 10 °CA ATDC; each T_{2c}-KL_{2c} image pair is from a different engine cycle.

from the endoscope and presents a long flame pathway L, which is thought to explain the large KL_{2c} values found in this region.

3.2. Discussion on interpretations from 2C data and uncertainties

For each of the four crank angles introduced in Fig. 6, 50 instantaneous images of the two wavelengths were captured from sequential cycles to build up an ensemble. For each calculated T_{2c}-KL_{2c} image-pair that resulted from the 2C images, the soot radiance levels were considered so that sources of erroneous data could be eliminated. These errors may have been the result of aspects such as camera noise, or obstruction of optical components such as the endoscope window. Figure 8 provides a distribution map of the T_{2c} and KL_{2c} pixel values calculated from one cycle, captured at 10 °CA, plotted in T_{2c}-KL_{2c} space. The solid black lines represent equally spaced soot radiance curves with labelled ra-

diance values, whereby any T_{2c}-KL_{2c} combination along that line would give the same light emission to the endoscope at 650 nm. Also shown in dotted lines are the minimum and maximum possible light emission from the combination of cameras used, taking the most restrictive value from either the 550 nm or 650 nm channel; the upper line relates to the camera saturation value and the lower line relates to the mean camera background signal value.[2] It is seen that flame locations with a lower soot KL_{2c} value must have a higher temperature to give the same radiance as soot with a higher KL_{2c} value. The effect of soot KL_{2c} value becomes less important as KL_{2c} increases, particularly above $KL_{2c} = 1.5$.

The algorithm used to calculate T_{2c} and KL_{2c} simultaneously truncates the KL_{2c} value at 3 during iteration for calculation efficiency, since at this point the emissivity is already around 0.999, and the KL_{2c} value at such points tends to continue to rise indefinitely without further influencing the temperature value.
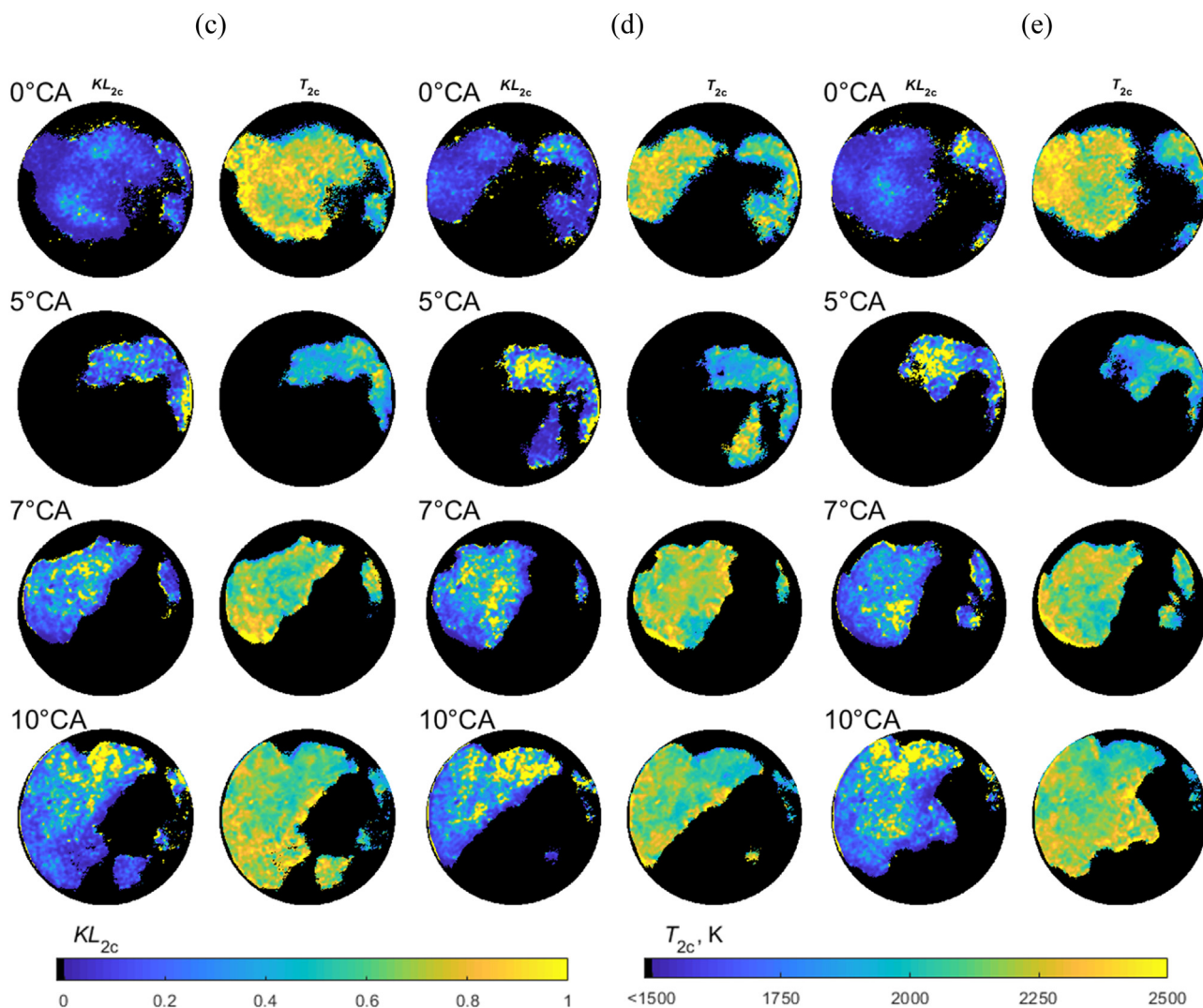
Fig. 7. Continued

A mean T_{2c}-KL_{2c} map for all valid (eliminating erroneous data that fall below the noise threshold) data from the set of 50 images was built by binning the T_{2c}-KL_{2c} space. These are presented in Fig. 9(a) for the crank angles analysed in this study. In Fig. 9(b), the mean T_{2c}-KL_{2c} map for 10 °CA is presented again, with contours of constant signal-noise ratio, showing that a majority of the data points have a signal-noise ratio above 10.

The pilot injection flame, shown in the 0 °CA image, shows a flame with low soot quantity represented by the low KL_{2C} values, accompanied by a higher flame temperature. The peak (modal) T-KL pair is at $T_{2C} = 2425$ K and $KL_{2C} = 0.025$.

The main combustion begins around 4–5 °CA, which is shown by the overall low light levels given by the 5 °CA T_{2c}-KL_{2c} plot, which encroaches on the background-light limit (Fig. 9(a) top-right) giving a low signal-to-noise ratio. The 5 °CA and 0 °CA T_{2c}-KL_{2c} maps are similar in shape, with the 5 °CA map showing an increase in locations with a higher soot KL_{2c} and lower temperature. The 5 °CA images show a flame with a smaller penetration and area than those at 0 °CA. However, the higher KL_{2c} values show that there is already a greater amount of soot produced in the flame at this stage compared with the pilot injection. The modal temperature and KL values rise for 7 °CA and 10 °CA as the combustion proceeds towards a short-lived steady-state phase before the end of injection.

3.3. Average T and KL interpretation

To analyse the flame behaviour at each crank angle, a mean from the ensemble of 50 calculated T_{2C} and KL_{2C} images was calculated. For temperature images, due to variability in the flame location and the fact that zero signal (i.e. no sooting flame) does not correspond to zero temperature (0 K), simply taking the mean results is an unrealistic representation of the mean flame temperature distribution. A selective average was chosen where, for each pixel, the mean was calculated only from cycles when there was flame data identified on that cycle. To reduce the contribution from outliers for visualization and comparison to simulation, an occurrence threshold of 10 out of 50 cycles was used before pixels were selected to contribute to this mean image. Together these images allow an understanding of the mean temperature field. For KL_{2c}, a mean of the 50 images may be performed as zero KL_{2c} does represent no soot. The mean images ensemble-averaged in this way are shown in Fig. 10 for the same timings introduced in Fig. 7.

The temporal development of mean flame temperature and soot KL_{2c} obtained from the 2C technique are plotted in Fig. 11a (data from condition discussed above, at 1400 rpm - load 1), and in Fig. 11b of results from two additional operating conditions (Fig. 11b): at the same engine speed with a higher (doubled) load condition (load 2, in red), and at the same load (load 1) but a
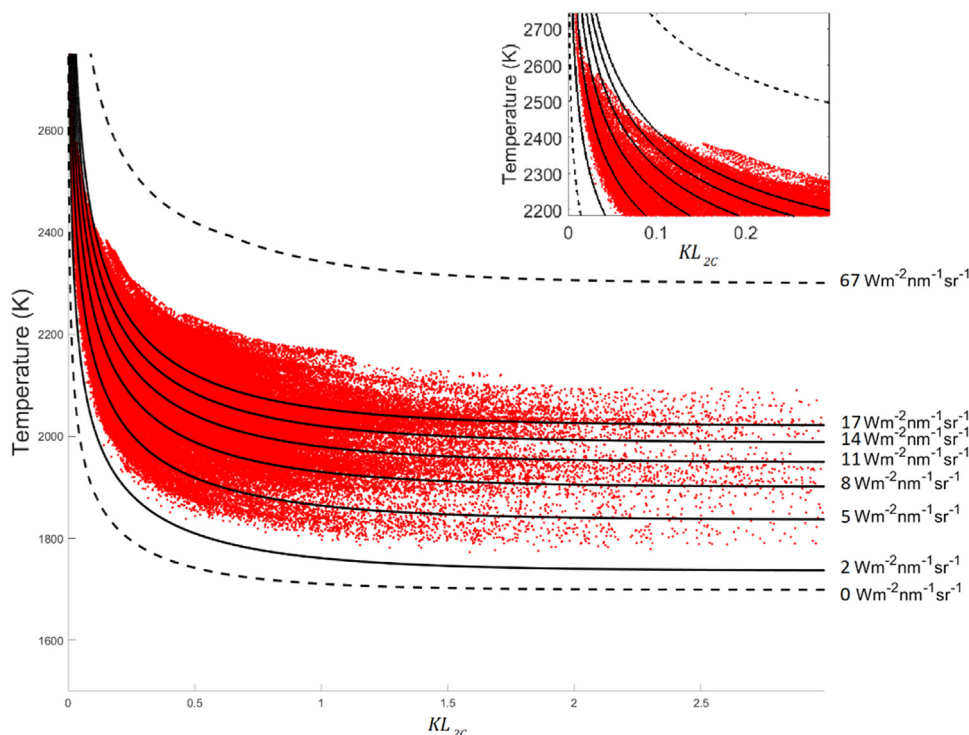
Fig. 8. T_{2c}-KL_{2c} Map for 10 °CA ATDC for one instantaneous 2C acquisition, showing families of light intensity curves (solid and dash lines) at 650 nm. The dashed lines at 0 Wm^{-2}nm^{-1}sr^{-1} and 67 Wm^{-2}nm^{-1}sr^{-1} correspond to the mean camera background signal[1] and the camera saturation value respectively.

higher engine speed (in blue) The profiles of the cylinder pressure, AHRR, and the injector current of the higher speed condition are plotted in Fig. 11b as a reference. At 1400 rpm, load 1 (Fig 11a, black), T_{2c} (solid symbol) for the pilot combustion peaks after that of the AHRR (solid line) and before soot KL_{2C} (empty symbol) peaks ~10 °CA. As for the main combustion event, both T_{2C} and KL_{2C} indicate a dip where AHRR peaks. This is likely due to limitation in the field-of-view of the collection optics (the endoscope), where the flame propagates outside the visible area. Similar trends are seen for the other two conditions.

To understand better where combinations of temperature and soot concentration are distributed within the combustion chamber, Fig. 12 shows physical locations of calculated T_{2c} and KL_{2c} from two interesting ranges of values for the data captured at 10 °CA. These ranges are shown in the red and black circle in Fig. 12(a) and are at a similar levels of light intensities and signal-noise ratios. The distribution of the relatively high T_{2c}, low KL_{2C} regions is around the flame edges and towards the lower side of the nearest plume – Fig. 12(b) top. The distribution of relatively low T_{2c}, high KL_{2C} regions is mainly towards the centre of the nearest plume but also towards the top of the image, representing flames at the far side of the combustion chamber – Fig. 12(b) bottom. This seems to support the basic assumptions about likely flame structure, as shown in Fig. 4, but is compounded by the overlapping flames and the non-orthogonal viewing angle. The overlap of the two plumes nearest to the injector (Plumes 1 and 2) will act to extend the path length L, thus reducing the inferred soot concentration from measured values of KL_{2c}. Further modelling would be required to quantify whether this has significant effect on the T_{2c} and KL_{2c} measurements and flame structure inferred from them.

Higher measured values of KL_{2c} (greater than 1) are expected to suffer from significant uncertainty, as shown in Fig. 3. Very high instantaneous measured KL_{2C} are found in regions without great temperature variation, typically as a local peak in KL_{2C}, potentially due to contribution from camera noise. At values of KL_{2C} greater than 0.5, there is only minor effect of further increasing KL_{2C}, as

demonstrated by the lines of constant light intensity in Fig. 8. Therefore, regions of KL_{2C} greater than 0.5 are interpreted as high soot regions.

3.4. Application of T-KL flim

To relate the 2C measurements to information and understanding about the physical flame structure, this section applies the flame light intensity model, described in Section 2.5, to the 10 °CA data. Considering the flame structure reported for single plume investigations [9], the soot radiance from locations towards the edge of the 2-D image of the plume is expected to correspond to a line-of-sight through predominantly high temperature, relatively low soot regions, where the equivalence ratio is closest to unity. Conversely, soot radiance from pixels located close to the spray axis will have travelled along a path through both the high temperature, low soot regions and through the flame core, where soot levels are expected to be higher and temperatures lower due to the higher equivalence ratio. To begin to quantify what the actual temperature distribution between the flame edge and the flame centreline is, sets of parameterized temperature and soot ($k_{soot}L$) distributions (shown in Eq. (15)) have been fitted to two T_{2C}-KL_{2C} datapoint pairs, for the case at 10 °CA. These correspond to data typical of the flame edge and the flame centreline respectively, as represented in Fig. 12(b). The chosen values used were calculated from the average temperature and KL images generated as described earlier: T_{2C} = 2200 K and KL_{2C} = 0.1 to represent the flame edge and T_{2C} = 1950 K and KL_{2C} = 0.65 to represent the flame at the spray axis. The soot radiance at these representative T_{2C} and KL_{2C} combinations are within 10% of each other at 650 nm, using Eq. (1). For the flame centreline, where there is also an increased frequency of higher KL_{2C} values in relatively uniform temperature regions, the same temperature value was tested with the increased KL_{2C} value of 1.5 to assess whether these large KL_{2C} values are meaningful variations in flame soot, which could be fully or partially attributed to actual variations in the measured flames. The

(a)

(b)
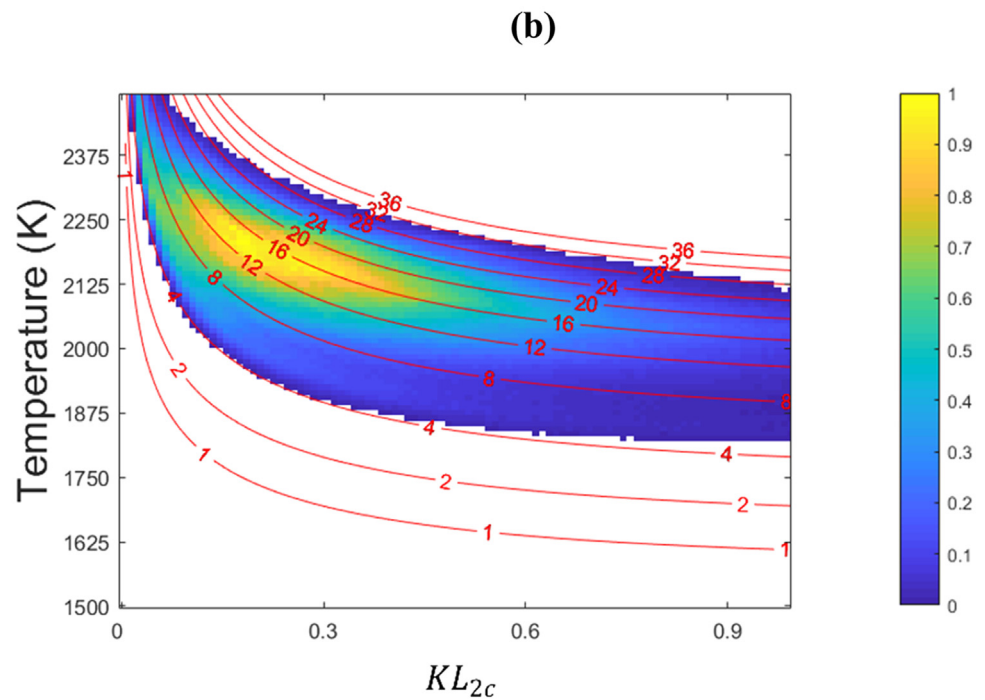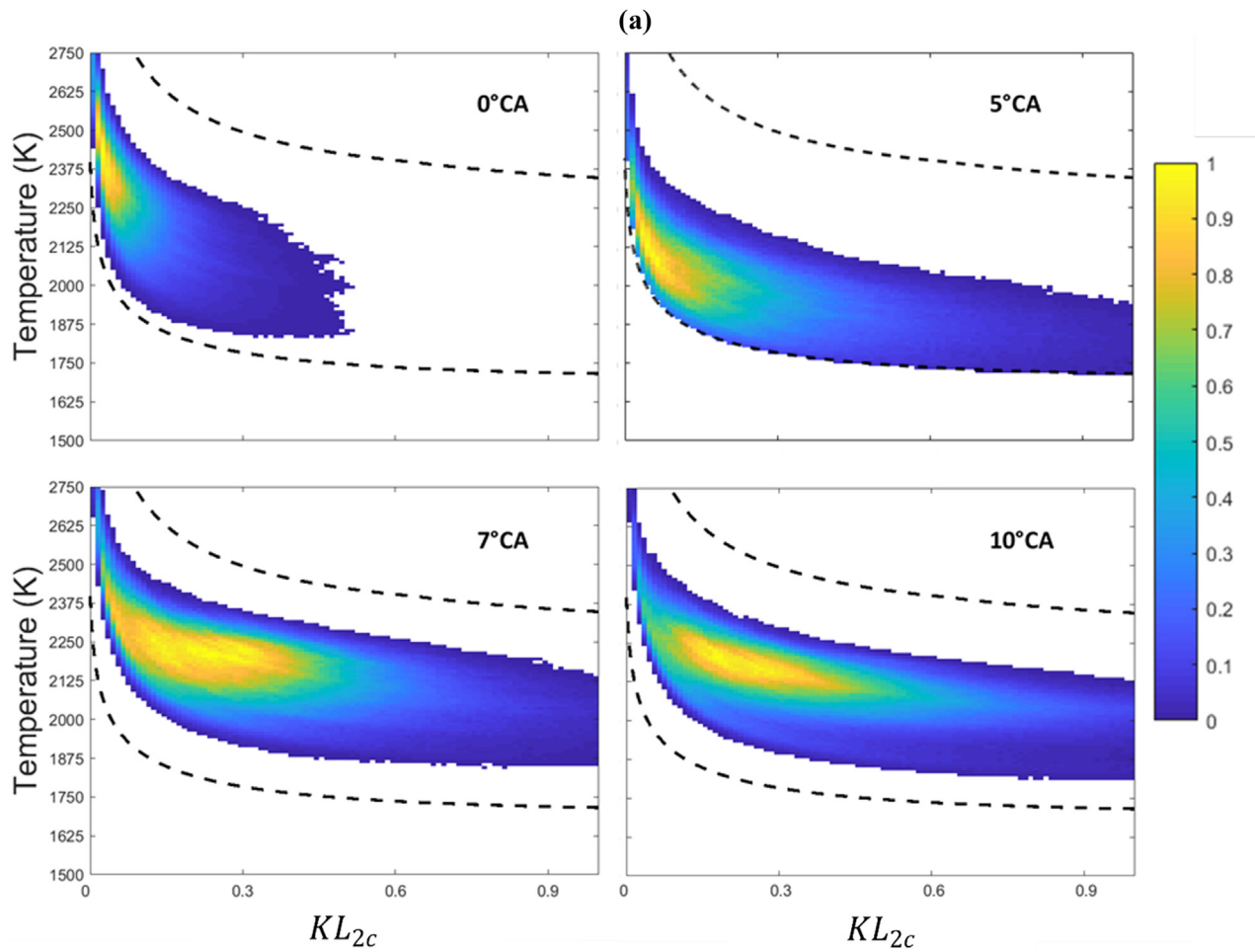
Fig. 9. (a) Normalized frequency maps in T_{2c}–KL_{2c} space showing the distribution across the set of 50 images at each crank angle studied. The dashed lines are the background light level line and the maximum signal line which relates to the camera saturation value, respectively. (b) Contour map of signal-noise ratio overlaid over 10 °CA T_{2c}-KL_{2c} frequency map, showing that majority of datapoints are in the region of 12–20 signal-noise ratio and 63% have a signal-noise ratio greater than 10.
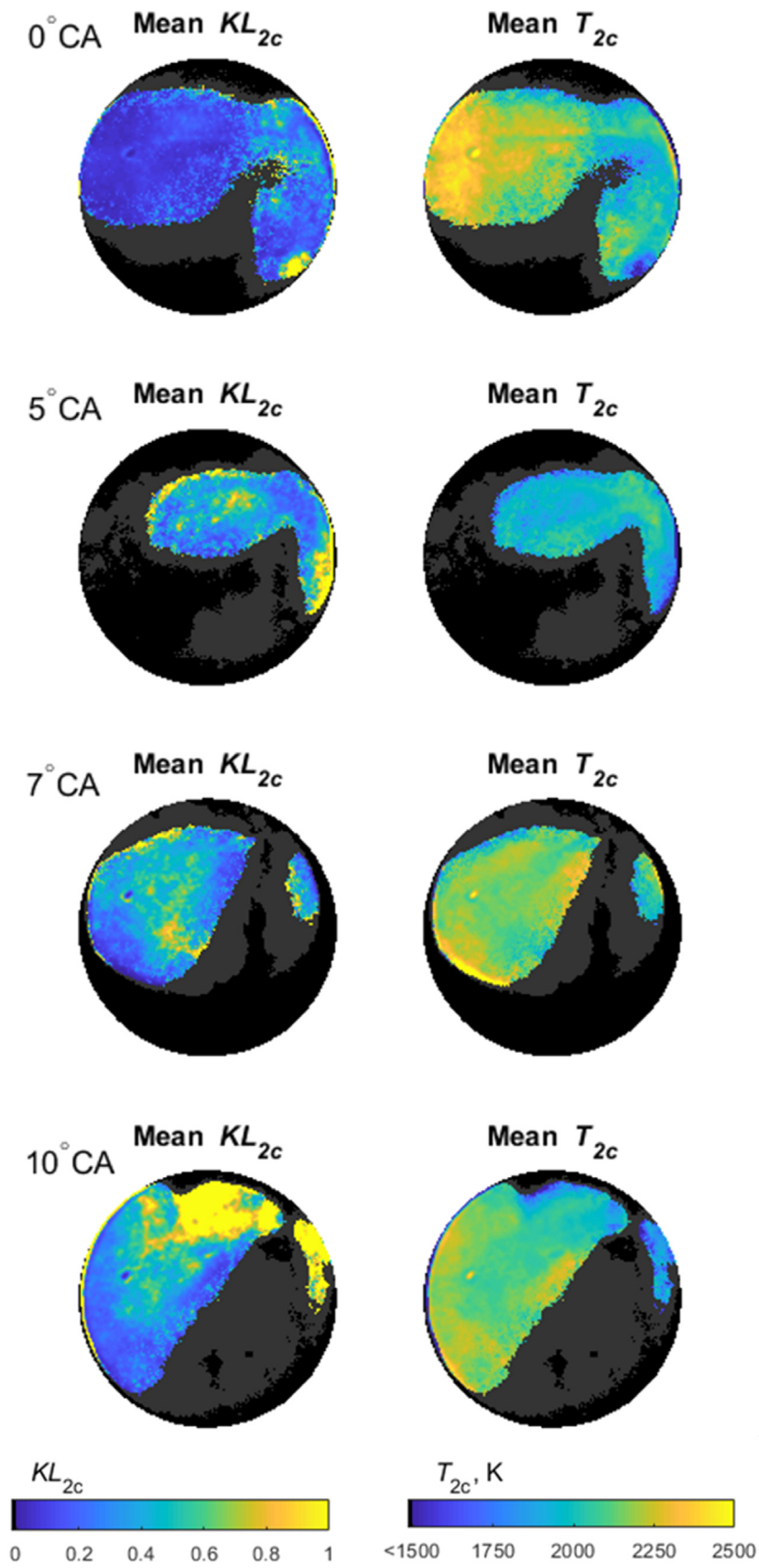
Fig. 10. Ensemble-averaged T_{2c} and KL_{2c} images at 0 °CA, 5 °CA, 7 °CA and 10 °CA ATDC, from 50 cycles - the grey regions represent regions excluded from visualization as described in the text.
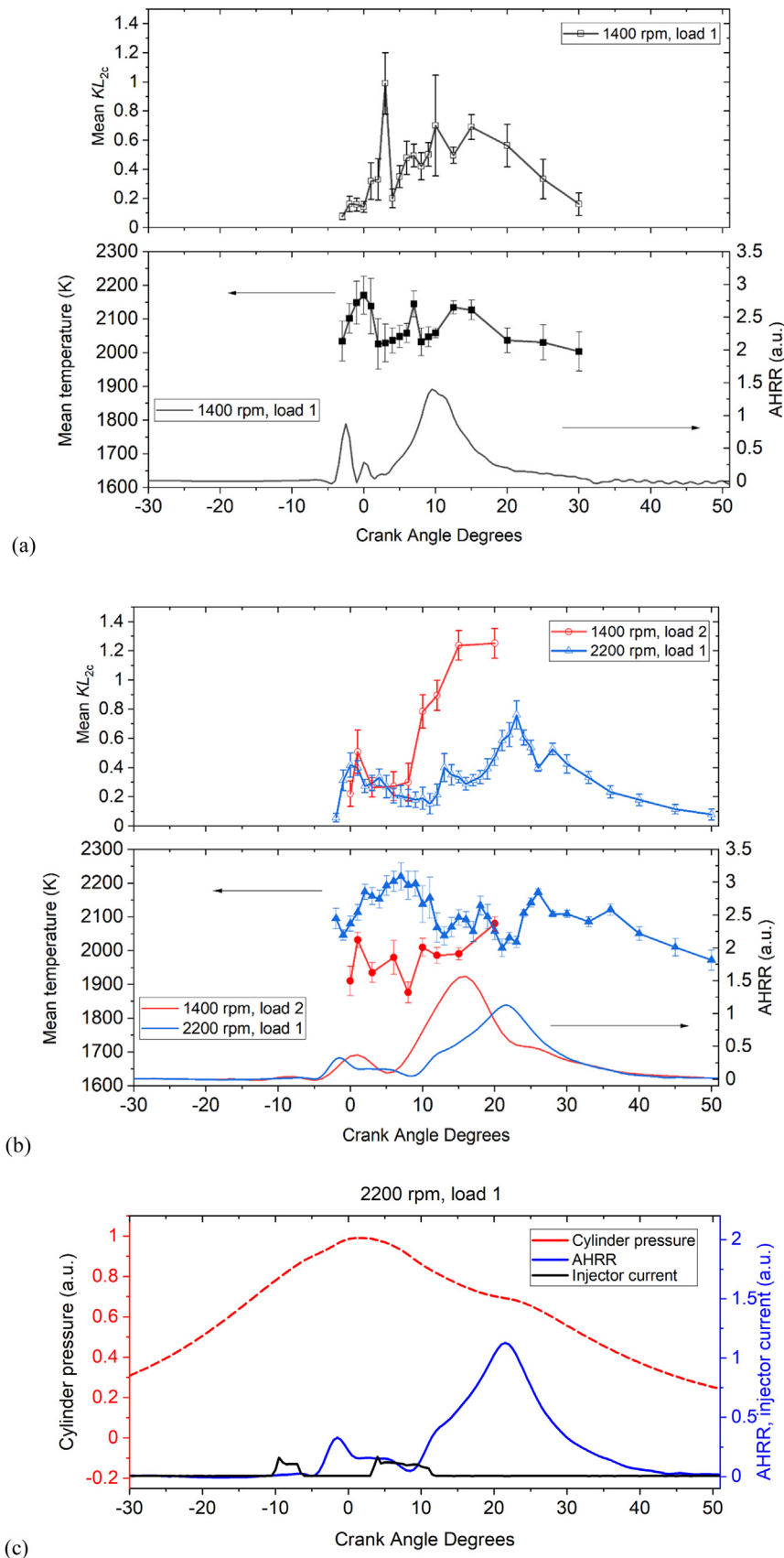
Fig. 11. (a, b) The two-colour field-of-view averaged soot KL_{2C} (top) and temperature (bottom) calculated from the ensemble-averaged T_{2C} and KL_{2C} images, plotted with apparent heat release rate (AHRR) derived from the simultaneously-acquired ensemble-averaged cylinder pressure. Error bars indicate one standard deviation either side of mean, across the 50 cycles[2]. Data from three operating conditions are shown: (1) 1400 rpm – load 1, in black, (2) 1400 rpm – load 2, in red, and (3) 2200 rpm – load 1, in blue. (c) Profiles of measured cylinder pressure (a.u.), calculated AHRR (a.u.) and injector current (a.u.) at the higher speed condition.

(a) (b) (c)
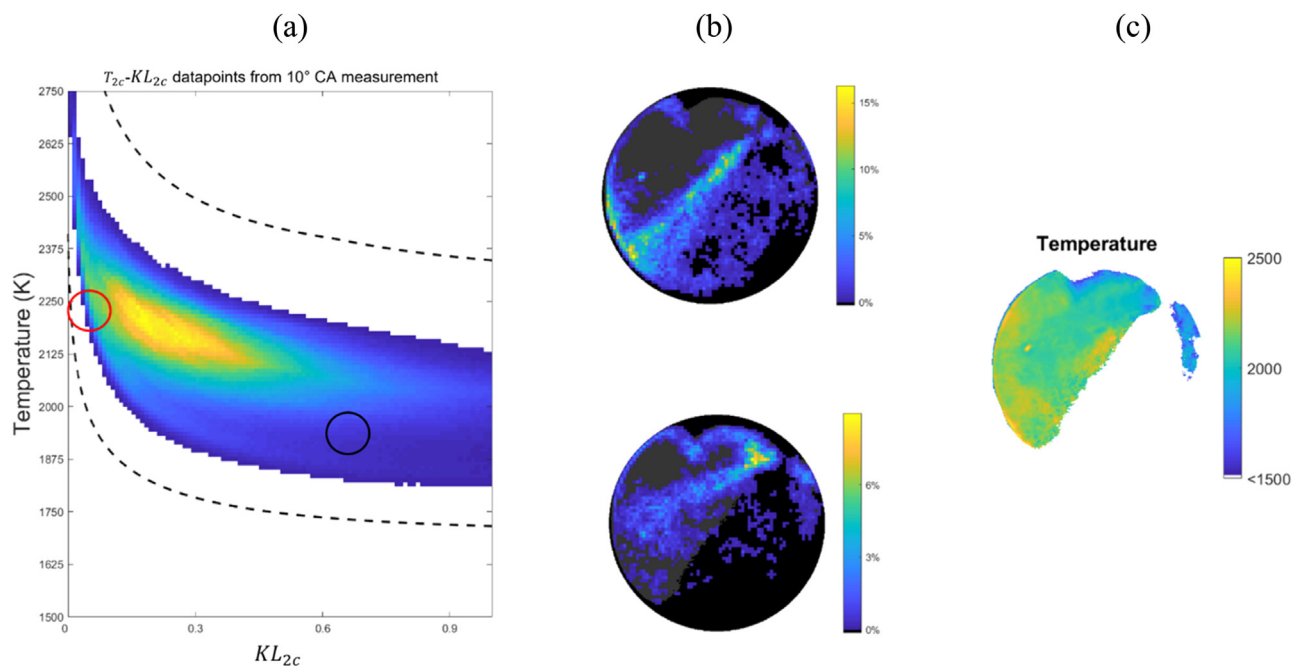
Fig. 12. (a) Measured T_{2c}-KL_{2c} combinations for all 50 images taken at 10 °CA, with two interesting T_{2c}-KL_{2c} sub-sets highlighted: (red circle) $T_{2C} = 2180 - 2275$ K, $KL_{2C} = 0 - 0.1$; and (black circle) $T_{2C} = 1895 - 1990$ K, $KL_{2C} = 0.6 - 0.7$. (b) Top: the physical locations of red-circle marked sub-set of the 2C measured data, and the corresponding percentage occurrence; bottom: physical locations and the corresponding occurrence of the black-circled sub-set of 2C measured data. Superimposed is the envelope of the ensemble-averaged image (in grey), representing an occurrence of more than 10 out of 50 cycles. (c) The 'ensemble-averaged' temperature image at 10 °CA.

process is discussed next and the outcome of increasing the value KL_{2C} to 1.5 at the flame centreline is shown in Fig. 13(b).

Given a distribution of temperature T_i and soot $k_{soot,i}L$, Eq. (11) can be used to generate what the temperature and soot KL would be if analysed with the 2C method. Calculation proceeded by assigning a k_{soot} distribution, of type shown in Fig. 4(a), and performing an optimization to see if there exists a linear three-point temperature distribution, of type shown in Fig. 4(a) and Fig. 5, that produced the same 2C temperature and KL factor as the 2C measurements. The family of $k_{soot}L$ distributions investigated uses a five-point distribution (expressed in Eq. (15)) with low $(k_{soot}L)_e$ at the edge and variable $(k_{soot}L)_c$ and $(k_{soot}L)_q$ at both the centreline and quarter-point (mid-way between centreline and edge). The value of $(k_{soot}L)_e$ was limited to $k_{soot}L < KL_{2C}$ and the centreline and quarter-point values limited to $k_{soot}L < 2 KL_{2C}$.

Figure 13 presents the temperature and soot distributions responsible for the minimum and maximum flame edge temperature possible given the limits adopted, along with the 2C values for comparison. As expected, the minimum flame edge temperature generated, within the k_{soot} bounds investigated, was equal to the corresponding 2C temperature. Many other linear temperature distributions were found within the maximum and minimum flame edge temperature, with corresponding soot distributions within the parameters described previously. For distributions with low or zero k_{soot} at the flame edge (peak temperature zone), the flame edge temperature was always above the 2C temperature. In general, for a constant overall KL_{2C}, an increased soot concentration throughout the flame requires a reduced flame centreline temperature (where k_{soot} is largest), resulting in a corresponding increased flame edge temperature in order to achieve the required T_{2C}.

For the flame edge measurement location, distributions shown in Fig. 13(a) ($T_{2C} = 2200$ K and $KL_{2C} = 0.1$), the maximum centreline $k_{soot}L$ value, for which any temperature distribution existed that allowed a match with the 2C measured data, was 0.2. This generated a flame edge temperature of 2520 K and a flame centreline temperature of 1770 K along the line-of-sight at this location.

Further increasing $k_{soot}L$ values in the centre of the distribution above the imposed limits of $k_{soot}L < 2 KL_{2C}$ slightly increases the maximum temperature to a peak of 2630 K, which requires a flame centreline temperature below 1000 K. This bounding distribution will depend on the choice of distribution shape. Since the minimum flame edge temperature along the line-of-sight was equal to the 2C measurement, this places the bounds for flame edge temperature at 2200–2630 K, corresponding to a 430 K or 19.6% uncertainty interval.

However, at this location, where the temperature and soot concentration distribution are anticipated to be more uniform along the line-of-sight, there can be more confidence in the feasible temperature distributions that are more uniform. Distributions studied here with uniform or near-uniform temperature have temperature values close to the 2C measured value of 2200 K.

For the flame centreline 2C measurement location ($T_{2C} = 1950$ K and $KL_{2C} = 0.65$), the path length will be longer than at the flame edge. A non-uniform temperature distribution, with a reduction in the centre is expected to be most realistic. In Fig. 13(b), the maximum flame edge temperature is 2130 K and the flame centreline temperature is at 1730 K. Further increasing the local $k_{soot}L$ beyond the prescribed limits of $2 KL_{2C}$ for this combination of T_{2C} and KL_{2C} does not in fact increase the maximum temperature. As discussed earlier, there are regions within the 2C images where there is increased KL_{2C}. In these regions, where KL_{2C} can increase to 1.5 at constant 2C temperature, the maximum flame edge temperature leading to a feasible temperature distribution is reduced to 2000 K and the overall span of temperatures throughout the thickness of the flame reduces. This is a potential contribution to the explanation of localized high KL measurements.
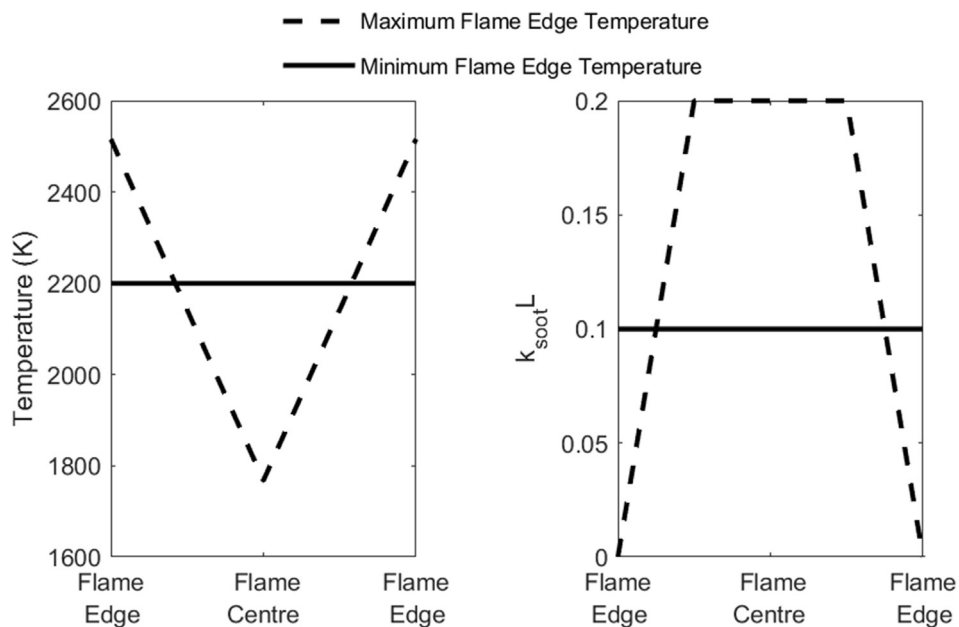
3.5. Analysis of flim results

These sample comparisons between measurements from the 2C imaging and consideration of the structure of the flame temperature and soot profile allow some upper bounds to be put
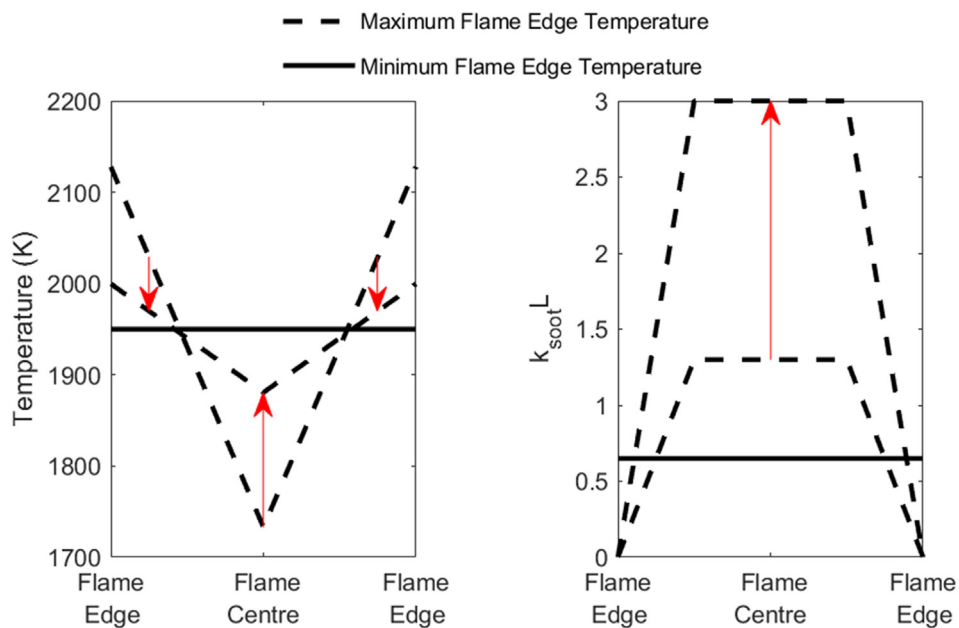
Fig. 13. Feasible combinations of T-$k_{soot}L$ distributions along line-of-sight showing extremes of flame edge temperature (greatest and smallest): (a) typical flame edge location with $T_{2C} = 2200$ K, $KL_{2C} = 0.1$; (b) typical flame centreline location with $T_{2C} = 1950$ K and $KL_{2C} = 0.65$ and $KL_{2C} = 1.5$ (shift in distributions when KL_{2C} increased to 1.5 is shown by red arrow). The minimum temperatures also correspond exactly with the 2C temperatures.
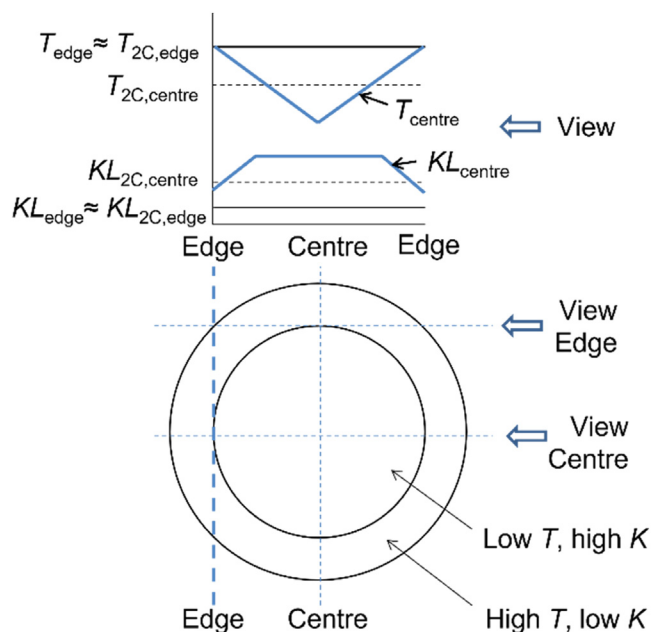
Fig. 14. Idealized developed flame (at 10 °CA ATDC) soot *KL* and temperature distribution and flame cross section, showing relationship between edge and centreline measurements and edge and centreline real distributions.

on the possible uncertainty due to the line-of-sight nature of the technique. However, this uncertainty is dependent on the assumed flame structure and shape, and the minimum centreline and maximum edge-flame temperatures that are accepted as physical. Figure 14, shows a schematic of an axisymmetric flame structure with the two views corresponding to locations analysed in Fig. 13 superimposed. Due to the unsteady nature of the flame and non-orthogonal viewing angle, a full 3-D tomographic reconstruction is not attempted but the schematic serves to illustrate the consistency of the 2C measurements made at different parts of the flame, as an attempt to reduce the uncertainty in knowledge of the flame structure.

For the flame edge measurement location, it is expected that conditions will be uniform, meaning $T_{edge} \approx T_{2C,edge}$ and $KL_{edge} \approx KL_{2C,edge}$ as found in Fig. 13(a), for the distribution with minimum flame edge temperature. In principle, the flame edge temperature T_{edge} found along this line-of-sight should correspond closely with the edge temperature of T_{centre} that is found along the line-of-sight through the plume centre, as shown in the graph in Fig. 14. From Fig. 13(a), this was between 2200 K and 2630 K. The maximum T_{edge} calculated for the view through the plume centre was found to be 2130 K, which puts more confidence in edge temperatures closer to the 2200 K lower bound. The *KL* values from the two measurement locations are less likely to correspond well with each other, since in both cases they will tend to zero at the edge of the flame.

An analytical calculation of the adiabatic flame temperature, T_{ad}, of the in-cylinder flame was performed at the same operating condition using the cylinder pressure, fluids temperatures and air/fuel ratio parameters. The estimated adiabatic flame temperature is around 2700 K, which is slightly higher than the temperature range (at 2200 K – 2630 K of flame edge) obtained from the FLIM model and the T_{2C} data shown previously, for example, in Fig. 10. This is as expected given that the heat loss was not taken account of in the calculation of the T_{ad}, and shows that 2C measured temperature and the possible true flames' temperature range derived by the FLIM are reasonable and performed well.

4. Conclusions and future work recommendations

This paper assesses the practical application of the two-colour soot pyrometry for in-cylinder diesel flame temperature and soot concentration measurements, including evaluation of the technique uncertainties and evaluation of self-consistent temperature and soot concentration distributions along the line-of-sight. An endoscopic access system for acquisition of data from simultaneous optical diagnostic techniques from a production diesel engine has been introduced. Two-colour soot pyrometry using two intensified cameras obtained temperature and soot *KL* factor maps of the spray flames, which can provide additional understanding of the in-cylinder combustion process and data for future model validation. The measurement uncertainties were discussed in detail including the errors introduced from the optical setup, calibration process, and the detector responses. A line-of-sight flame light intensity model (FLIM) was built and applied to the 2C data to further understand the uncertainties from the line-of-the-sight nature of the 2C technique. The FLIM is of a type previously used but the application here considers three new aspects: non-orthogonal views through the flame; consideration of the effects of finite flame thickness; use of the model to back-calculate a plausible temperature and soot concentration distribution in a real flame. This has aided the interpretation of the *T* and *KL* results from this engine, and will contribute to more robust CFD model validation in industrial applications.

The overall uncertainty of the two-colour technique due to method and instrumentation was estimated at less than 5.5% in T_{2C} and 34–97% in KL_{2C} (for the range of $0 < KL < 1$), before account is taken of the line-of-sight nature of the technique or finite flame thickness. The effect of finite flame thickness was found to reduce the estimate of the peak temperature (near the flame edge) by up to 100 K. The varying uncertainty values for *KL* are found because of the logarithmic relationship between measured flame radiation intensity and *KL*, as described in Eq. (4). For calibration of the optical system for *KL* measurement, the best estimate of the calibration constant is important but reducing uncertainty in this value will not significantly reduce uncertainty in the *KL* measurements. For the datasets studied in this paper, between 89% and 96% of all the flame pixels measured had a *KL* value less than 1. *KL* measured values above 1 are subject to considerable uncertainty, regardless of the accuracy of the calibration experiment, and do not offer any additional interpretation of flame soot concentration or effect on flame temperature.

Means of presenting the ensemble data from the 2C diesel flame images have been explored and presented, considering the cycle-to-cycle variations of the flames. In particular, presentation of the measured values in T_{2c}-KL_{2c} space, incorporating measurements from the whole ensemble, has allowed identification of the ranges of soot concentration and temperature that are present in that flame. An ensemble average was performed on a pixel basis, only from cycles when there was data measured at that pixel on that cycle. For visualization and comparison to simulation, an occurrence threshold of 10 out of 50 cycles was used before pixels were selected to contribute to this mean image.

By applying the FLIM proposed, internal temperature and soot distributions can be compared to the point measurements from the two-colour technique. Trial T_{2C}-KL_{2C} pairs were compared with results from the FLIM to understand further uncertainties from the in-cylinder diesel flames due to the line-of-sight nature of the technique. Initially, the range in possible flame-edge temperatures could be over 300 K, when using the FLIM on a line-of-sight through the flame centre, as shown in Fig. 13(a). However, when this information was compared to the expected distribution, and to T_{2C} values calculated from a line intersecting closer to the flame

edge, greater confidence was given that the actual flame-edge temperature at that location is close to the lower side of the range. In context of Fig. 13(a), this means flame edge temperature is closer to 2200 K than to 2500 K, which is a decrease in the measurement uncertainty, due to the application of the FLIM as described in this paper. In the context of CFD model validation, this increases the usefulness of the technique for quantitative comparisons with simulation results, such as comparison of temperature radial profile.

In short, although the 2C measurement is an aged technique, it still required further attention to better support its practical applications such as in the diesel engine combustion diagnostic. This work assessed the applicability in diesel engine combustion study: limitations (line-of-sight, finite flame thickness), uncertainties (in T_{2C} and KL_{2C}), and mitigations (developed a FLIM model accounting the flame thickness effect, and back-calculating a plausible flame T and KL distributions from the measured 2C data). The paper provided in-depth discussions and recommendations for CFD validation activities, thus has considerable and long-term contribution to support industry research and development.

Further modelling work and comparison to experimental results is recommended to assess the impact on measured values of neglecting the variation in flame distance to detector and of multiple diesel flame plumes along the line-of-sight.

Declaration of Competing Interest

The authors declare that they have no known competing financial interests or personal relationships that could have appeared to influence the work reported in this paper.

Acknowledgments

References

[1] T. Kamimoto, H. Kobayashi, Combustion processes in diesel engines, Prog. Energy Combust. Sci. 17 (1991) 163–189.

[2] M.P.B. Musculus, L.M. Pickett, In-cylinder spray, mixing, combustion, and pollutant-formation processes in conventional and low-temperature-combustion diesel engines, In: Zhao, H (ed.) Advanced direct injection combustion engine technologies and development. Cambridge: Woodhead Publishing Limited (2010) pp. 644–675.

[3] S.A. Skeen, J. Manin, L.M. Pickett, E. Cenker, G. Bruneaux, K. Kondo, T. Aizawa, F. Westlye, K. Dalen, A. Ivarsson, T. Xuan, J.M. Garcia-Oliver, Y. Pei, S. Som, W. Hu, R.D. Reitz, T. Lucchini, G. D'Errico, D. Farrace, S.S. Pandurangi, et al., A progress review on soot experiments and modeling in the engine combustion network (ECN), SAE Int. J. Engines 9 (2) (2016) 883–898.

[4] Y. Matsui, T. Kamimoto, S. Matsuoka, A study on the time and space resolved measurement of flame temperature and soot concentration in a D I diesel engine by the two-color method, SAE Technical Paper 790491, 1979.

[5] H.C. Hottel, F.P. Broughton, Determination of true temperature and total radiation from luminous gas flames: use of special two-color optical pyrometer, Ind. Eng. Chem. - Anal. Ed., 4 (1932) 166–175.

[6] B.C. Connelly, S.A. Kaiser, M.D. Smooke, M.B. Long, M. Eng, N. Haven, Two-dimensional soot pyrometry with a color digital camera, 4th Joint Meeting U.S. Section of the Combustion Institute, 2005.

[7] F.R.A. Jorgensen, M. Zuiderwyk, Two-colour pyrometer measurement of the temperature of individual combusting particles, J. Phys. E 18 (1985) 486–491.

[8] B. Ma, G. Wang, G. Magnotti, R.S. Barlow, M.B. Long, Intensity-ratio and color-ratio thin-filament pyrometry: uncertainties and accuracy, Combust. Flame 161 (2015) 908–916.

[9] S. Skeen, J. Manin, L. Pickett, K. Dalen, et al., Quantitative spatially resolved measurements of total radiation in high-pressure spray flames, SAE Technical Paper 2014-01-1252, 2014.

[10] D.R. Snelling, G.J. Smallwood, F. Liu, Ö.L. Gülder, W.D. Bachalo, A calibration-independent laser-induced incandescence technique for soot measurement by detecting absolute light intensity, Appl. Opt. 44 (2005) 6773–6785.

[11] G.J. Smallwood, A critique of laser-induced incandescence for the measurement of soot PhD Thesis, Cranfield University, 2008.

[12] H. Zhao, B. Williams, R. Stone, Measurement of the spatially distributed temperature and soot loadings in a laminar diffusion flame using a cone-beam tomography technique, J. Quant. Spectrosc. Radiat. Transf. 133 (2014) 136–152.

[13] D.R. Snelling, K.A. Thomson, G.J. Smallwood, O.L. Guider, E.J. Weckman, R.A. Fraser, Spectrally resolved measurement of flame radiation to determine soot temperature and concentration, AIAA J. 40 (9) (2002).

[14] T. Yu, F.J. Bauer, F.J. Huber, S. Will, W. Cai, 4D temperature measurements using tomographic two-color pyrometry, Opt. Express 29 (4) (2021) 5304–5315.

[15] J. Vattulainen, V. Nummela, R. Hernberg, J. Kytölä, A system for quantitative imaging diagnostics and its application to pyrometric in-cylinder flame-temperature measurements in large diesel engines, Meas. Sci. Technol. 11 (2000) 103–119.

[16] C. Beatrice, C. Bertoli, N.C. Cirillo, N. Del Giacomo, S.D. Stasio, Two-colour pyrometry measurements of soot loading in a diesel engine burning model fuels of varying quality, Combust. Sci. Technol. 110–111 (1995) 321–339.

[17] J.J. López, J. Martín, A. García, D. Villalta, A. Warey, Implementation of two color method to investigate late cycle soot oxidation process in a CI engine under low load conditions, Appl. Therm. Eng. 113 (2017) 878–890.

[18] M.P.B.B. Musculus, S. Singh, R.D. Reitz, Gradient effects on two-color soot optical pyrometry in a heavy-duty DI diesel engine, Combust. Flame 153 (2008) 216–227.

[19] M. Bakenhus, R.D. Reitz, Two-color combustion visualization of single and split injections in a single-cylinder heavy-duty DI diesel engine using an endoscope-based imaging system, in: SAE Technical Paper 1999-01-1112, 1999.

[20] X.R. Li, W. Yang, L.M. Zhao, F.S. Liu, The influence of pilot-main injection matching on DI diesel engine combustion using an endoscopic visualization system, Fuel 188 (2017) 575–585.

[21] M. Khosravi, P. Kirchen, Refinement of the two-color pyrometry method for application in a direct injection diesel and natural gas compression-ignition engine, Proc. IMechE Part D: J. Automob. Eng. 233 (14) (2019) 3787–3800.

[22] F. Payri, J.V. Pastor, J.M. García, J.M. Pastor, Contribution to the application of two-colour imaging to diesel combustion, Meas. Sci. Technol. 18 (2007) 2579–2598.

[23] Oriel product training - Solar Simulation, 2006, available via: https://www.newport.com/medias/sys_master/images/images/h9c/hea/8797264445470/Solar-Simulation.pdf.

[24] H. Zhao, N. Ladommatos, Optical diagnostics for soot and temperature measurement in diesel engines, Prog. Energy Combust. Sci. 24 (1998) 221–255.

[25] R. Hessel, Z. Yue, R. Reitz, M. Musculus, J. O'Connor, Guidelines for interpreting soot luminosity imaging, SAE Int. J. Engines 10 (2017).

[26] Steady Flame Burner, from Yale coflow diffusion flames, available via: http://guilford.eng.yale.edu/Yalecoflowflames/burners.html.

[27] Report of calibration of one standard of spectral irradiance (250–2400 nm), Newport Corp, 2016.

[28] J.R. Taylor, An introduction to error analysis the study of uncertainties in the physical measurements, 1982.

[29] S.A. Skeen, K. Yasutomi, E. Cenker, B. Adamson, N. Hansen, L.M. Pickett, Standardized optical constants for soot quantification in high-pressure sprays, SAE Int. J. Engines 11 (2018) 805–816.

[30] S.S. Pandurangi, M. Bolla, Y.M. Wright, K. Boulouchos, S.A. Skeen, J. Manin, L.M. Pickett, Onset and progression of soot in high-pressure n - Dodecane sprays under diesel engine conditions, Int. J. Engine Res. 18 (2017) 436–452.